Pro Gradu

Surface plasmon polariton interaction with Sulforhodamine 101 dye

Svitlana Baieva

University of Jyväskylä

Nanoscience center

Department of physics

8th of April, 2011

Abstract

The integration of conventional optical elements and electronic circuits is limited by size mismatch between these components. The diffraction limit does not allow miniaturizing optical elements to nm-scale. It was realized that light being strongly coupled to coherently oscillating electrons at the metal surface could be used to overcome this limit. The coupled state is called surface plasmon polariton. Surface plasmon polariton propagates in plane of metallic film within 10-100 μm range but decay exponentially in perpendicular directions to metal-dielectric boundary. Interaction of the surface plasmon polaritons with fluorescent dye molecules may result in development of new nanodimensional photonic elements as planar frequency converters, planar refractive elements with desirable refractive index *etc*. Conversion from light to the surface plasmon polariton modes and backwards can be done employing fluorescent molecules. Due to imperfections of metallic film surface plasmon polariton can be scattered into photons that can excite fluorescent molecules. One of the most powerful techniques of the surface plasmon polaritons propagation imaging is based on this effect. The study of surface plasmon polaritons interaction with fluorescent dye molecules is high priority task.

The aim of this thesis is an investigation of the interaction between surface plasmon polaritons and Sulforhodamine 101 dye molecules. The fundamental property of SPP oscillation is dispersion relation: the dependence of energy of oscillation on the wave vector of the oscillation. The dispersion curves for silver-Sulforhodamine 101 samples are obtained experimentally performing reflectometry measurements. Excitation is done by using prism coupling technique (Kretschmann configuration). The vacuum Rabi splitting is observed. Transfer matrix method is used to model reflection coefficient R of studied multilayer structures. Detection of the scattered radiation provides another way to get dispersion relation of surface plasmon polaritons. Comparison of this dispersion relation to one obtained from reflectometry measurements provides insight into dynamics of surface plasmon polariton/dye molecules interaction.

Contents

1. Introduction

In recent decades the attention has been paid to experimental and theoretical study of exciton and photon interaction phenomena in quantum microcavities [1, 2, 3]. The quantum microcavity is usually formed by alternate layers of high and low refractive index semiconducting materials – distributed Bragg reflector (DBR). The cavity usually has width equal to the desirable wavelength that is formed between the DBRs. Quantum microcavity permits control of photonic and excitonic properties. Resonant wavelength is controlled by cavity thickness; while the width of the resonance is determined by cavity thickness as well as the refractive indices of the materials that form the cavity. Excitonic properties can be changed by placing quantum wells (QW) into the cavity. The typical materials used for DBRs formation are $Al_xGa_{1-x}As$ compounds, $In_xGa_{1-x}As$ can be used for QWs and cavity material could be GaAs [1]. The most of the work in this area is based on axial confinement by the DBRs, including the study of the dispersion of cavity polaritons, Rabi oscillations observation, bleaching of the strong coupling, and control by changing external conditions (temperature, electric, magnetic fields) [1].

In order to obtain a significant interaction between the cavity photon and excitonic state in QW, the excitonic energy should be resonant with cavity mode. The strong coupling manifests itself in this case by anticrossing behavior of the dispersion curve and is called Rabi splitting by analogy with atom-photon interaction considered by Rabi [4]. The coupling is determined by exciton oscillator strength and the amplitude of the electromagnetic field associated with cavity mode and can be described by energy difference between the branches of the dispersion curve

$$E_{Rabi} = 2\hbar\left(\frac{2\Gamma_0 c N_{qw}}{n_c L_{eff}}\right)^{1/2}, \tag{1.1}$$

where c is the speed of light, n_c is refractive index of the cavity material, L_{eff} is an effective cavity length, N_{qw} is the number of QWs and $\hbar\Gamma_0$ is the radiative width of the free exciton. It can be expressed in terms of exciton oscillator strength per unit area f_{ex}

$$\hbar\Gamma_0 = \frac{\pi}{n_c}\frac{e^2}{4\pi\varepsilon_0}\frac{\hbar}{m_e c} f_{ex}, \tag{1.2}$$

where e and m_e are electron charge and mass, ε_0 is the vacuum dielectric constant.

Also in-plane dispersion of such cavities was studied in [5, 6]. In-plane wave vector component is not quantized in this case and in-plane dispersion can be determined. In the study of *Houdré et al.* [5] the angle of incident light was fixed. Collecting emitted light at different angles the dispersion curves were obtained. The energy split was obtained to be *7.6* meV for *29º* angle of incidence, when the measurements was done at *77* K. *Baxter et al.* obtained dispersion relation for quantum microcavity by varying light incidence angle; the energy split was also observed [6].

Also a huge attention has been paid to the surface plasmons, which are coherent oscillations of electron plasma at metal-dielectric boundary. Their interaction with light has been studied very efficiently since 1960s [10, 11]. Many unexpected phenomena were observed during these years [12, 13, 14]. For example, *Ebessen et al.* [13] demonstrated a strong enhancement of transmitted light through periodic 2D-arrays of holes in a metallic film with dimensions smaller than the wavelength. The polarization dependence, dependence on the incidence angle and dependence on the film material prove that the enhancement is a result of light coupling to the surface plasmons.

The size mismatch between conventional optic devices (due to diffraction limit these components cannot have size smaller than several wavelengths) and electronic components (size range is 100 nm -100 μm) does not allow their integration into effective optoelectronic circuits. But the light being coupled to surface plasmons can be confined into sub-μm scale [15, 16]. The idea of light propagation in a form of surfce plasmon polaritons (SPPs) inspired many research groups to develop new types of waveguides [15], light to surface plasmon polariton convertors [17], planar optical components [18] and many others.

Also the key role of SPPs in optical metamaterials was realized. Metamaterials are structures possessing properties that are not present in natural materials, but are designed by introducing different structural elements. Electromagnetic metamaterials are characterized by unusual electromagnetic properties, such as negative magnetic permittivity and negative refractive index. For example, the SPP planar waveguides were used to achieve negative refraction in visible frequencies [19]. *Atwater et al.* fabricated Au-Si_3N_4-Ag waveguide sustaining a SPP mode with antiparallel group and phase velocities. At visible frequency range $\omega_{SP}^{Ag-Si_3N_4} < \omega < \omega_P^{Au}$ (where $\omega_{SP}^{Ag-Si_3N_4}$ and ω_P^{Au} are the resonant frequencies of Ag-Si_3N_4 SPPs

and the Au bulk plasmons) the dispersion curve of SPP mode exhibits negative slope ($\frac{dE}{dk_x} < 0$). For such a multilayer structure in double-prism configuration geometry the refractive index was deduced from the Snell's law to be $n(\lambda = 514nm) = -4.6$.

Interaction of SPPs with fluorescent dye molecules (organic semiconductors) may result in development of new nanodimensional photonic elements. Conversion from light to SPP modes and backwards can be done employing fluorescent molecules [17, 20]. Due to imperfections of a metallic film surface SPPs can be scattered into photons that can excite fluorescent molecules. Also SPPs can excite fluorescent molecules directly. One of the most powerful techniques of SPPs propagation imaging is based on this effect.

The behavior of in-plane dispersion of the exciton – cavity photon interaction discussed above is very similar to behavior of dispersion relation of surface plasmon polariton – exciton interaction [7]. However, to achieve surface plasmon polariton – exciton strong coupling no optical cavity is needed. A typical sample is prepared on a glass substrate. The thin metal layer is evaporated on the substrate and as in [7, 8] organic semiconductor layer is formed on the top. The organic semiconductors (cyanide dye J-aggregates, Rhodamine 6G *etc.*) have large oscillator strength, so in principal huge Rabi splitting can be achieved (equations 1.1, 1.2). The energy splits for planar structures having an organic semiconductor were obtained to be up to *200* meV for Rhodamine 6G dye [8]. But the large exciton linewidth that is due to vibronic states and inhomogeneous broadening complicates observation of strong coupling regime in quantum microcavities [9].

Taking into account a variety of applications for structures based on SPPs interaction with fluorescent dye molecules in weak and strong coupling regimes the study of dynamics of these interactions is high priority task.

In this work the SPP dispersion curves for silver-Sulforhodamine 101 fluorescent dye samples are obtained experimentally by performing reflectometry measurements.

Sulforhodamine 101 dye is widely used in biological imaging to monitor Ca^{2+} amount in the medium. This organic semiconductor has two absorption maxima at around *550* and *600* nm and large oscillator strength (section 4.3). So it is a good candidate to achieve a large Rabi splitting. SPPs excitation is done by prism coupling technique (Kretschmann configuration). Due to the similarity to exciton-cavity photon coupling the formalism of the vacuum Rabi

splitting is easily adapted to explain SPP dispersion relation behavior. Results obtained from a coupled oscillator model and transfer matrix method are in good agreement with experimental data. Detection of the scattered radiation provides another way to get dispersion relation of SPPs. Comparison of this dispersion relation to one obtained from reflectometry measurements provides insight into dynamics of the SPPs/dye molecules interaction [8].

2. Theoretical approaches to the analysis of surface plasmon polaritons

2.1. Surface plasmon polariton is a result of the Maxwell equations

The free electrons can fluctuate coherently on a metal boundary. These oscillations are called surface plasmons. As a result of interaction between surface plasmon and light in strong coupling regime the quasiparticle called surface plasmon polariton (SPP) can be formed. The SPP is a coupled state of conductor's electron plasma and electromagnetic field (figure 2.1.1 a)). The electromagnetic field has a maximum at the surface ($z=0$) and it is localized in the z direction within the Thomas-Fermi screening length (figure 2.1.1 b)). The field can be described by

$$E = E_0^{\pm} \exp[+i(k_x x \pm k_z z - \omega t)], \qquad (2.1.1)$$

for $z \geq 0$ one should take + and for $z \leq 0$ one should take –. The imaginary k_z causes exponential decay of E_z. $k_x = \frac{2\pi}{\lambda_p}$ is parallel to the x direction and λ_p is the wavelength of the plasma oscillation.

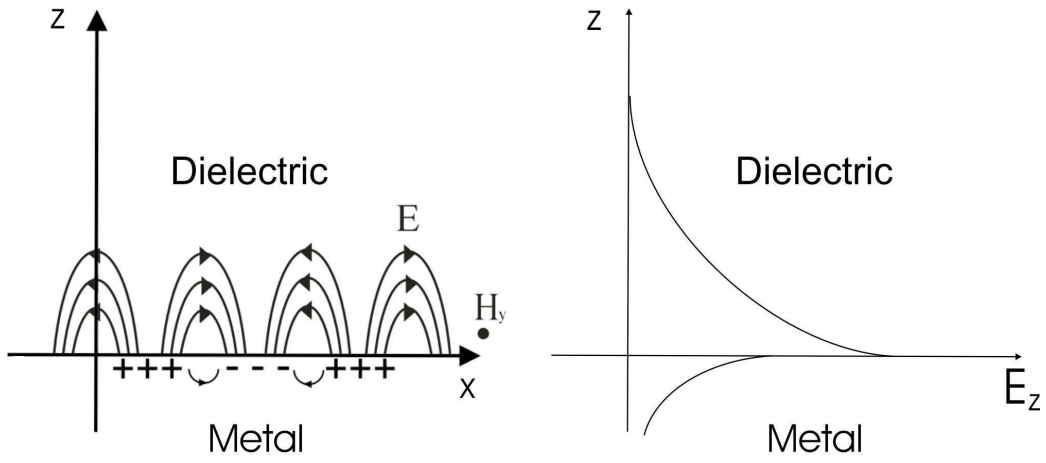

a) b)

Figure 2.1.1 a) Schematic picture of the electromagnetic field and charges that are associated with SPP; b) Exponential decay of E_z in dielectric and metal layers.

A fundamental property of the SPP oscillation is its dispersion relation, *i.e.*, the dependence of frequency (or energy) of longitudinal oscillation on wave vector of the oscillation. The simplest case of SPPs is oscillation on a surface of a semi-infinite metal. The system is shown on figure 2.1.2.

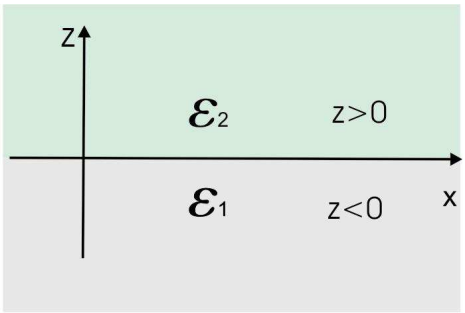

Figure 2.1.2 Schematic picture of interface between two layers.

First consider *p*-polarized (TM polarization) electromagnetic wave that propagates in the x direction along the interface between the metal, which is described by complex dielectric permittivity $\varepsilon_1 = \varepsilon_1(\omega) = \mathrm{Re}[\varepsilon_1(\omega)] + i\,\mathrm{Im}[\varepsilon_1(\omega)]$, and the dielectric with $\varepsilon_2 = \varepsilon_2(\omega) = \mathrm{Re}[\varepsilon_2(\omega)] + i\,\mathrm{Im}[\varepsilon_2(\omega)]$ [21]. The field is not dependent on y coordinate and can be written as

$$z > 0 \qquad H_2 = (0, H_{y2}, 0)\exp[i(k_{x2}x + k_{z2}z - \omega t)],$$

$$E_2 = (E_{x2}, 0, E_{z2})\exp[i(k_{x2}x + k_{z2}z - \omega t)]; \tag{2.1.2}$$

$$z < 0 \qquad H_1 = (0, H_{y1}, 0)\exp[i(k_{x1}x - k_{z1}z - \omega t)],$$

$$E_1 = (E_{x1}, 0, E_{z1})\exp[i(k_{x1}x - k_{z1}z - \omega t)]. \tag{2.1.3}$$

The set of Maxwell's equations that must be fulfilled is

$$\nabla \times H_{1,2} = \varepsilon_{1,2}\frac{1}{c}\frac{\partial}{\partial t}E_{1,2}, \tag{2.1.4}$$

$$\nabla \times E_{1,2} = -\frac{1}{c}\frac{\partial}{\partial t}H_{1,2}, \tag{2.1.5}$$

$$div\varepsilon_{1,2}E_{1,2} = 0, \tag{2.1.6}$$

$$divH_{1,2} = 0 \tag{2.1.7}$$

and boundary conditions that must hold at $z = 0$ are

$$E_{x1} = E_{x2}, \tag{2.1.8}$$

$$H_{y1} = H_{y2}, \tag{2.1.9}$$

$$\varepsilon_1 E_{z1} = \varepsilon_2 E_{z2}, \tag{2.1.10}$$

(2.1.8) and (2.1.9) result in

$$k_{x1} = k_{x2} = k_x . \tag{2.1.11}$$

From equation (2.1.4) one gets

$$k_{z1} H_{y1} = \frac{\omega}{c} \varepsilon_1 E_{x1},$$

$$k_{z2} H_{y2} = -\frac{\omega}{c} \varepsilon_2 E_{x2} . \tag{2.1.12}$$

The equations (2.1.12), (2.1.8) and (2.1.9) give the system of uniform linear equations

$$H_{y1} - H_{y2} = 0,$$

$$\frac{k_{z1}}{\varepsilon_1} H_{y1} + \frac{k_{z2}}{\varepsilon_2} H_{y2} = 0; \tag{2.1.13}$$

and the determinant of the system is

$$\frac{k_{z1}}{\varepsilon_1} + \frac{k_{z2}}{\varepsilon_2} = 0 . \tag{2.1.14}$$

And one gets (2.1.12) by solving equations (2.1.4), (2.1.5)

$$k_x^2 + k_{z1,2}^2 = \varepsilon_{1,2} (\frac{\omega}{c})^2 . \tag{2.1.15}$$

Finally by combining (2.1.14) and (2.1.15) the dispersion relation for SPPs at the boundary of two semi-infinite media is obtained

$$k_x = \frac{\omega}{c} \sqrt{(\frac{\varepsilon_1 \varepsilon_2}{\varepsilon_1 + \varepsilon_2})} . \tag{2.1.16}$$

Figure 2.1.3 represents the energy ($E = \hbar\omega$) of the SPP as a function of $\mathrm{Re}[k_x]$ (a) and as a function of $\mathrm{Im}[k_x]$ (b) for semi-infinite metal layer and semi-infinite air layer ($\varepsilon = 1$). In general case $k_x = \mathrm{Re}[k_x] + i\,\mathrm{Im}[k_x]$ and $E = \mathrm{Re}[E] + i\,\mathrm{Im}[E]$. In optical region the relations for wave vector and energy the following relations are usually hold

$$\mathrm{Im}[k_x] << \mathrm{Re}[k_x]$$

$$\mathrm{Im}[E] << \mathrm{Re}[E] . \tag{2.1.17}$$

But in some cases the uncertainty in wave vector can be large (figure 2.1.3) and the limits of a well-defined wave vector should be considered [22]. In the regions, where the relations (2.1.17) are fulfilled, one considers the SPP's dispersion relation as $E = E(\mathrm{Re}[k_x])$.

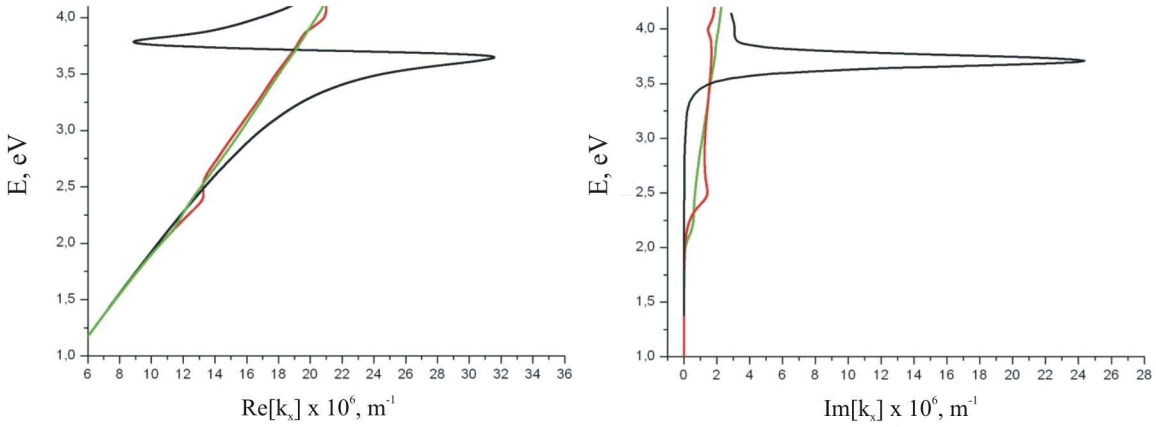

a) b)

Figure 2.1.3 a) Energy as a function of $\mathrm{Re}[k_x]$; b) energy as a function of $\mathrm{Im}[k_x]$. Black curve represents semi-infinite silver layer/semi-infinite air layer structure; red curve represents semi-infinite gold layer/semi-infinite air layer structure; green curve represents semi-infinite copper layer/semi-infinite air layer structure. The permittivities of the metals are calculated using the refractive index and media damping coefficients presented in [23].

It can be shown that the values k_{z1} and k_{z2} are imaginary, so the field amplitude decreases exponentially normal to surface. According to [11] the skin-depth, *i.e.* the length within which the field decreases e^{-1} times, is

$$l_{skin1,2} = \frac{1}{|k_{z1,2}|}. \tag{2.1.18}$$

For the silver layer and air one gets skin-depth to be equal to 23 nm and 370 nm, respectively, for the wavelength of 600 nm; and, 29 nm, 280 nm for gold and air interface for the same wavelength (data for silver and gold dielectric permittivities are taken from [23]).

Consider also the possibility to excite SPPs with *s*-polarized field (TE polarization). In this case the field is described as

$$z > 0 \qquad H_2 = (H_{x2}, 0, H_{z2}) \exp[i(k_{x2}x + k_{z2}z - \omega t)],$$

$$E_2 = (0, E_{y2}, 0) \exp[i(k_{x2}x + k_{z2}z - \omega t)]; \tag{2.1.19}$$

$$z < 0 \qquad H_1 = (H_{x1}, 0, H_{z1}) \exp[i(k_{x1}x - k_{z1}z - \omega t)],$$

$$E_1 = (0, E_{y1}, 0) \exp[i(k_{x1}x - k_{z1}z - \omega t)]. \tag{2.1.20}$$

Continuity of H_x and E_y results in the relation

$$k_{1z} + k_{2z} = 0. \tag{2.1.21}$$

But $\mathrm{Im}[k_{1z}] > 0$ and $\mathrm{Im}[k_{2z}] > 0$, so the condition (2.1.21) cannot be fulfilled. Thus it is impossible to excite SPPs with *s*-polarized electromagnetic field.

The first approach to real systems is the SPPs that propagate on a thin metallic film in an asymmetric environment. The system is shown on figure 2.1.4.

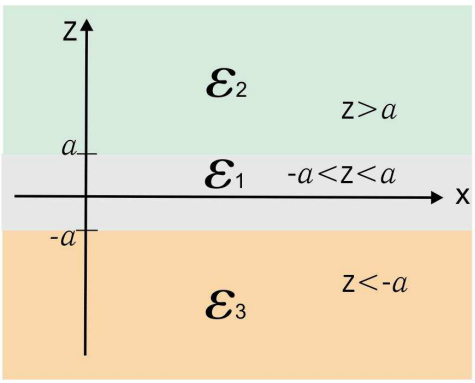

Figure 2.1.4 Schematic picture of three layers structure.

The electromagnetic field in this case is

$z < -a$

$$H_3 = (0, H_{y3}, 0)\exp[i(k_{x3}x + k_{z3}z - \omega t)],$$
$$E_3 = (E_{x3}, 0, E_{z3})\exp[i(k_{x3}x + k_{z3}z - \omega t)]; \tag{2.1.22}$$

$z > a$

$$H_2 = (0, H_{y2}, 0)\exp[i(k_{x2}x - k_{z2}z - \omega t)],$$
$$E_2 = (E_{x2}, 0, E_{z2})\exp[i(k_{x2}x - k_{z2}z - \omega t)]; \tag{2.1.23}$$

$-a < z < a$

$$H_1 = (0, H_{y1}, 0)\{\exp[i(k_{x1}x + k_{z1}z - \omega t)] + \exp[i(k_{x1}x - k_{z1}z - \omega t)]\}$$
$$E_1 = (E_{x1}, 0, E_{z1})\{\exp[i(k_{x1}x + k_{z1}z - \omega t)] + \exp[i(k_{x1}x - k_{z1}z - \omega t)]\} \tag{2.1.24}$$

Solving Maxwell's equations (2.1.4)-(2.1.7) together with two sets of boundary conditions (for *1/2* interface and *1/3* interface), the following dispersion relation can be obtained

$$\exp(4ik_{z1}a) = \frac{(\frac{k_{z1}}{\varepsilon_1} + \frac{k_{z3}}{\varepsilon_3})(\frac{k_{z1}}{\varepsilon_1} + \frac{k_{z2}}{\varepsilon_2})}{(\frac{k_{z1}}{\varepsilon_1} - \frac{k_{z3}}{\varepsilon_3})(\frac{k_{z1}}{\varepsilon_1} - \frac{k_{z2}}{\varepsilon_2})}. \quad (2.1.25)$$

And according to (2.1.15)

$$k_x^2 + k_{z1,2,3}^2 = \varepsilon_{1,2,3}(\frac{\omega}{c})^2. \quad (2.1.26)$$

In general case the equation (2.1.25) has to be solved numerically. Solving the Maxwell's equations one can get also an analytical expression for SPPs dispersion in multilayer systems. But it is challenging to solve these equations.

2.2. Reflectance of multilayer structures

The most common method in analyzing multilayer structure is the transfer matrix method [24]. Consider a *L*-layer structure presented in figure 2.2.1. Assume that the multilayer system is placed within a media with dielectric permittivity ε_0. The layers are homogeneous and isotropic, and are described by complex $\varepsilon_l = \varepsilon_l(\omega)$ (assume $\mu = 1$).

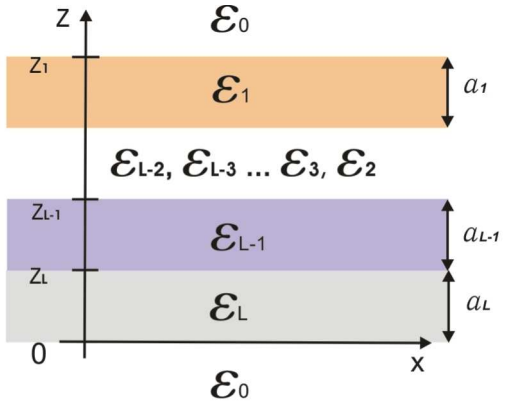

Figure 2.2.1 Schematic picture of *L*-layers structure.

A plane electromagnetic field is incident on the stack. Consider *p*-polarized light, *i.e.* the field is described by $H_{insident} = (0, H_y, 0)$. The field in l^{th} layer can be described as a superposition of two waves (reflected and transmitted waves)

$$H_l(x,z,t) = H_l^+(z)\exp[i(k_{xl}x + k_{zl}z + \omega t)] + H_l^-(z)\exp[i(k_{xl}x - k_{zl}z + \omega t)]. \quad (2.2.1)$$

As a result of transformation (reflection or transmission) across the interface between *l-1* layer and *l* layer the phase change occurs. It can be described as

$$\begin{pmatrix} H_l^{*+} \\ H_l^{*-} \end{pmatrix} = \begin{pmatrix} \phi_l^{-1} & 0 \\ 0 & \phi_l^{1} \end{pmatrix} \begin{pmatrix} H_{l-1}^{+} \\ H_{l-1}^{-} \end{pmatrix} = P_l \begin{pmatrix} H_{l-1}^{+} \\ H_{l-1}^{-} \end{pmatrix}, \quad (2.2.2)$$

$$\text{where } \phi_l = \exp[ik_{zl}a_l]. \quad (2.2.3)$$

On the other hand the change in amplitude and intensity can be described using Fresnel equations

$$\begin{pmatrix} H_l^{+} \\ H_l^{-} \end{pmatrix} = \begin{pmatrix} \frac{1}{t_{l,l-1}} & \frac{r_{l,l-1}}{t_{l,l-1}} \\ \frac{r_{l,l-1}}{t_{l,l-1}} & \frac{1}{t_{l,l-1}} \end{pmatrix} \begin{pmatrix} H_{l-1}^{+} \\ H_{l-1}^{-} \end{pmatrix} = A_l \begin{pmatrix} H_{l-1}^{+} \\ H_{l-1}^{-} \end{pmatrix}, \quad (2.2.4)$$

where

$$r_{l,l-1} = \frac{k_{zl}\varepsilon_{l-1} - k_{zl-1}\varepsilon_l}{k_{zl}\varepsilon_{l-1} + k_{zl-1}\varepsilon_l} \text{ and}$$

$$t_{i,l-1} = \frac{2k_{zl}\varepsilon_{l-1}}{k_{zl}\varepsilon_{l-1} + k_{zl-1}\varepsilon_l}. \quad (2.2.5)$$

Inserting (2.2.4) and (2.2.5) into the expression for matrix A_l and after simplification one gets

$$A_l = \frac{1}{2}\begin{pmatrix} 1 + \frac{k_{zl-1}\varepsilon_l}{k_{zl}\varepsilon_{l-1}} & 1 - \frac{k_{zl-1}\varepsilon_l}{k_{zl}\varepsilon_{l-1}} \\ 1 - \frac{k_{zl-1}\varepsilon_l}{k_{zl}\varepsilon_{l-1}} & 1 + \frac{k_{zl-1}\varepsilon_l}{k_{zl}\varepsilon_{l-1}} \end{pmatrix}. \quad (2.2.6)$$

Taking into account both change in the phase and in the amplitude one gets

$$\begin{pmatrix} H_l^{+} \\ H_l^{-} \end{pmatrix} = P_l A_l \begin{pmatrix} H_{l-1}^{+} \\ H_{l-1}^{-} \end{pmatrix} = T_l \begin{pmatrix} H_{l-1}^{+} \\ H_{l-1}^{-} \end{pmatrix} = \frac{1}{2}\begin{pmatrix} \exp[-ik_{zl}a] & 0 \\ 0 & \exp[ik_{zl}a] \end{pmatrix} \begin{pmatrix} 1 + \frac{k_{zl-1}\varepsilon_l}{k_{zl}\varepsilon_{l-1}} & 1 - \frac{k_{zl-1}\varepsilon_l}{k_{zl}\varepsilon_{l-1}} \\ 1 - \frac{k_{zl-1}\varepsilon_l}{k_{zl}\varepsilon_{l-1}} & 1 + \frac{k_{zl-1}\varepsilon_l}{k_{zl}\varepsilon_{l-1}} \end{pmatrix} \begin{pmatrix} H_{l-1}^{+} \\ H_{l-1}^{-} \end{pmatrix}. \quad (2.2.7)$$

To describe the total field transformation through the stack of L layers (that is described further by transformation matrix T) one has to take a product of L matrices of type T_l and take into account also the transformation through the surface $z_{L+1} = 0$. The dependence of reflected field H_r at $z_{L+1} = 0$ and transmitted field H_t at z_1 on incident field can be written as

$$\begin{pmatrix} H_{incident} \\ H_r \end{pmatrix}_{Z_{L+1}=0} = T\begin{pmatrix} H_t \\ 0 \end{pmatrix}_{Z_1} = \begin{pmatrix} T_{11} & T_{12} \\ T_{21} & T_{22} \end{pmatrix}\begin{pmatrix} H_t \\ 0 \end{pmatrix}_{Z_1}. \quad (2.2.8)$$

Then using a definition of reflection and transition coefficients for the stack

$$r_L = \frac{H_r(z=0)}{H_{insident}(z=0)},\ t_L = \frac{H_t(z=z_1)}{H_{incident}(z=0)}, \quad (2.2.9)$$

one can rewrite (2.2.8) as

$$\begin{pmatrix} 1 \\ r_L \end{pmatrix} = \begin{pmatrix} T_{11} & T_{12} \\ T_{21} & T_{22} \end{pmatrix}\begin{pmatrix} t_L \\ 0 \end{pmatrix} \quad (2.2.10)$$

and get

$$r_L = \frac{T_{21}}{T_{11}},\ t_L = \frac{1}{T_{11}}. \quad (2.2.11)$$

Reflectance (reflectance coefficient) can be found as

$$R = r_L r_L^* = \frac{T_{21}T_{21}^*}{T_{11}T_{11}^*}. \quad (2.2.12)$$

As an example consider a structure that consist of semi-infinite glass layer, 50 nm silver layer, 50nm dielectric resist layer with embedded Sulforhodamine 101 dye molecules and semi-infinite air layer. Glass is assumed to be dispersionless and have dielectric permittivity of 1.52^2. For silver dielectric permittivity one can use experimental data from *Johnson* and *Christie* [23]. The dielectric permittivity of the resist layer* is

$$\varepsilon(\omega) = 3 + \sum_{i=1}^{2} \frac{A_i \omega_{0i}^2}{\omega_{0i}^2 - \omega^2 - i\omega\gamma_i}, \quad (2.2.13)$$

where $A = \{0.133,\ 0.013\}$, $\omega_{0,i} = \{10.39,\ 11.33\}\ 10^6$ m^{-1} and $\gamma = \{1,\ 0.6\}\ 10^6$ m^{-1}. To model the dielectric permittivity function the classical theory of molecular dispersion has been used. In Appendix A one can find more details about the modeling.

The reflectance coefficient as a function of an incidence angle and a light wavelength of *p*-polarized light is plotted in figure 2.2.2. There are two strategies that can be used to get SPP's dispersion relation from this data. One can consider the white light incident on the structure

* In all examples in this thesis dielectric permittivity of Sulforhodamine 101 resist is obtained from measured transmittance of the reference sample. Its absorption is presented on figure 4.1.4, sample 4.

at a fixed angle. The reflectance coefficient as a function of wavelength will have several minima (in figure 2.2.2 red horizontal line represents such a measurement). Knowing the wavelength of the reflectance minima one can calculate the energy of SPP; knowing the angle of incidence and wavelength one can obtain in-plane component of the SPP's wave vector. The obtained dispersion relation of the structure is shown on figure 2.2.3 a) (black curve). In this case the strong coupling between SPP and dye molecule manifests itself as energy gaps. The SPPs possessing the frequencies that correspond to the Sulforhodamine 101 absorption maxima cannot be observed in the multilayer system. Mathematically, the resonant energy is a singularity point in the dispersion relation. SPP of resonant energy has infinitely large (if damping is neglected) wave vector component k_x.

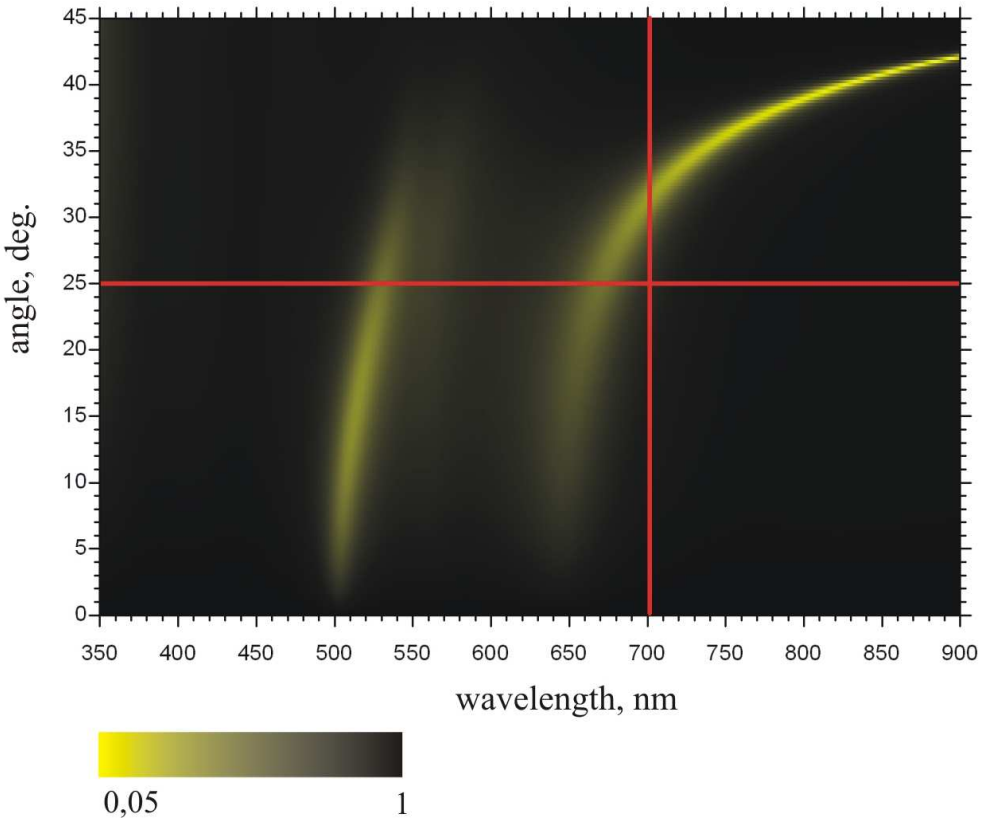

Figure 2.2.2 Reflectance coefficient of a multilayer structure (see text) as a function of incident angle and wavelength of *p*-polarized light.

The second strategy is illumination of the structure with a monochromatic light at different angles of incidence (in figure 2.2.2 red vertical line represents such a measurement).

In this case the reflectance coefficient as a function of the incidence angle has always only one minimum and dispersion relation looks like shown in figure 2.2.3 a) (red curve). The strong coupling regions are represented by the kinks on the dispersion curve. The uncertainty of wavevector component determination is very high at the kinks region. Figure 2.2.3 b) shows the reflection coefficient as a function of the angle at different excitation wavelengths. At wavelengths (e.g. *605* nm) close to the Sulforhodamine 101 absorbance maximum, the reflectance minimum gets wide and shallow. This huge uncertainty in the wavevector component means short lifetime of SPP. In this work the first type of the experiments was carried out.

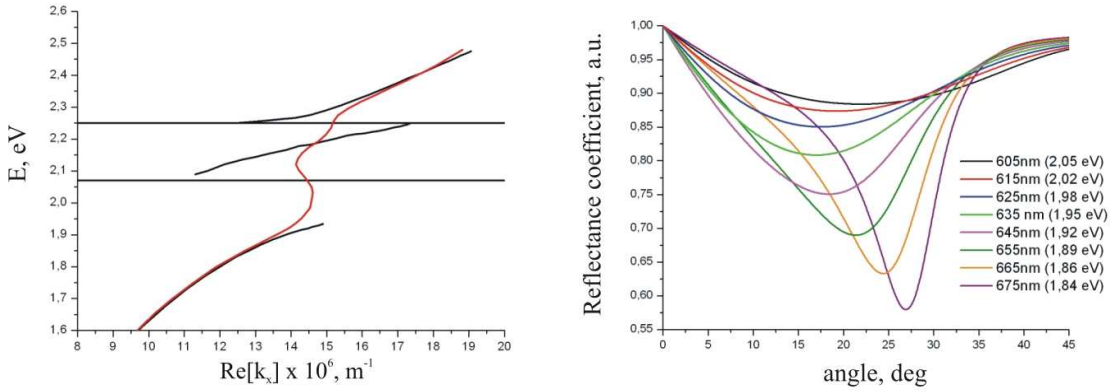

a) b)

Figure 2.2.3 a) Black curve is a dispersion function of multilayer structure (see text) obtained from experiment simulation with white light source and fixed angle of incidence; red curve is a dispersion function of the multilayer structure obtained from experiment simulation with monochromatic light source and changing the angle of incidence. Black horizontal lines represent the energies of Sulforhodamine 101 molecule excitons (absorbance maxima are at 2.07 eV (555 nm) and 2.25 eV (599 nm)). b) Reflectance coefficient as a function of light incidence angle. Curve colors mark the excitation wavelength that is written in the inset.

2.3. Theory of Rabi oscillations

As it was mentioned at the introductory part the concept of the Rabi splitting can be adapted to describe SPPs interaction with excitons. The origin of this concept is well-known Rabi problem [4]. It deals with electromagnetic wave interaction with two energy levels system.

Consider the electromagnetic wave that is resonant with a molecule transition frequency. As the result of interaction the molecule is excited from ground state. When a photon of the same frequency interacts with excited molecule, with certain probability it causes the emission of the photon, which has the same frequency and phase that initial electromagnetic field (stimulated emission). The regime described above is called a weak coupling regime. In this regime perturbation theory is valid and Fermi's Golden rule is applicable.

However, another regime can be achieved. If the coupling of the molecule and the electromagnetic field is high, the quasi-lossless strong coupling regime holds. The molecule absorbs and emits photon, due to the strong coupling the photon is absorbed again and re-emitted *etc*. This process is called Rabi oscillations. It is known that in this regime the system eigen states are mixed electron-photon states with an energy split that is dependent on square root of a transition oscillator strength, number of molecules and number of photons involved. When the number of photons is small this phenomenon is called the vacuum Rabi splitting [26]. The electronic states of the system and the electromagnetic field must be quantized to enter the strong coupling limit. So if a system has a continuum of electronic states no strong coupling effects occur and irreversible absorption is present.

One can fully describe system in a strong coupling regime by Jaynes -Cummings model. The electromagnetic field is quantized in this model. Here the semi-classical Rabi model is reviewed. In this model the system (atom or molecule) has quantized energy levels and the electromagnetic field is described as wave (classical description of electromagnetic field). The analogy to the SPP-exciton interaction problem can be easily made. SPP propagating at metal/dielectric matrix interface has certain oscillation frequency, this oscillation in reality is not monochromatic, but has a final linewidth. But within certain error one can think about this field as being monochromatic. Initial and final states of electronic transition in Sulforhodamine 101 are two levels under consideration.

In general case the Hamiltonian of the interacting system can be written as [4]

$$H = H_{mol} + H_{field} + H^{(I)}(t), \tag{2.3.1}$$

where H_{mol} is the free two level system (in present case Sulforhodamine 101 molecule) Hamiltonian, H_{field} is the Hamiltonian that describes the electromagnetic field and $H^{(I)}$ is the Hamiltonian that describes interaction between the atom and electromagnetic field.

The classical representation is used for field (for this problem we are not interested in magnetic component of electromagnetic field

$$E(t) = E_x(t) = E_0 Cos(\omega t). \tag{2.3.2}$$

Assume that the molecule can be in the ground state $|g>$ or in the excited state $|e>$. The free molecule Hamiltonian is

$$H_{mol} = \frac{1}{2}\hbar\omega_{eg}(|e><e| - |g><g|), \tag{2.3.3}$$

where $\omega_{eg} = \frac{E_e - E_g}{\hbar}$. Assume that the energy of the ground state is zero. In this case one can rewrite eq. (2.3.3) as

$$H_{mol} = \hbar\omega_{eg}|e><e|. \tag{2.3.4}$$

The interaction part of the Hamiltonian is

$$H^{(I)} = dE(t) = -dE_0 Cos(\omega t), \tag{2.3.5}$$

where dipole moment is $\vec{d} = -e\vec{r}$, e is electric charge. The Hamiltonian of interacting system is

$$H = \hbar\omega_{eg}|e><e| - dE_0 Cos(\omega t). \tag{2.3.6}$$

The state vector of the system is

$$C_g(t)|g> + C_e(t)\exp[-i(E_e - E_g)t/\hbar]|e> = C_g(t)|g> + C_e(t)\exp[-i\omega_{eg}t]|e>. \tag{2.3.7}$$

After inserting (2.3.7) in time-dependent Schrödinger equation

$$i\hbar\frac{\partial\Psi(t)}{\partial t} = H\Psi(t), \tag{2.3.8}$$

$$\begin{aligned} &i\hbar\frac{\partial}{\partial t}\{C_g(t)|g> + C_e(t)\exp[-i\omega_{eg}t]|e>\} = \\ &[\hbar\omega_{eg}|e><e| - dE_0 Cos(\omega t)][C_g(t)|g> + C_e(t)\exp[-i\omega_{eg}t]|e>] \end{aligned} \tag{2.3.9}$$

one can get equations for coefficients $C_g(t)$ and $C_e(t)$

$$\frac{dC_g}{dt} = \frac{-1}{i\hbar} E_0 Cos(\omega t) d_{eg} \exp[i\omega_{eg} t] C_e \tag{2.3.10}$$

$$\frac{dC_e}{dt} = \frac{-1}{i\hbar} E_0 Cos(\omega t) d_{eg}^* \exp[-i\omega_{eg} t] C_g , \tag{2.3.11}$$

where $d_{eg} = < e \mid d \mid g >$. The fact that at $t = 0$ only $\mid g >$-state is populated is used as initial conditions

$$C_g(0) = 1,\ C_e(0) = 0 . \tag{2.3.12}$$

After applying Rotating wave approximation (only slowly oscillating $(\omega_{eg} - \omega)$-terms are retained) one can get from (2.3.10) and (2.3.11)

$$\frac{dC_g}{dt} = 0 \tag{2.3.13}$$

$$\frac{dC_e}{dt} = \frac{i}{2\hbar} E_0 d_{eg}^* \exp[-i(\omega_{eg} - \omega)t] . \tag{2.3.14}$$

Solving the equations (2.3.13), (2.3.14) with initial conditions (2.3.12) and introducing

$$\Delta = \omega_{eg} - \omega , \tag{2.3.15}$$

one gets

$$C_e(t) = -i \frac{d_{eg}^* E_0}{\Omega_R \hbar} \exp[\frac{i\Delta t}{2}] Sin(\frac{\Omega_R t}{2}) , \tag{2.3.16}$$

$$\Omega_R = \sqrt{(\frac{d_{eg}^* E_0}{\hbar})^2 + \Delta^2} , \tag{2.3.17}$$

where Ω_R denotes the Rabi frequency.

Now the probability to find the system in the excited state can be calculated

$$P_e(t) = \mid C_e(t) \mid^2 = \frac{(d_{eg}^* E_0)^2}{(\Omega_R \hbar)^2} Sin^2(\frac{\Omega_R t}{2}) . \tag{2.3.18}$$

One can conclude that the smaller Δ the larger the probability of finding the molecule in the excited state. In the case of resonance, when $\omega_{eg} = \omega$, the Rabi frequency is directly proportional to the transition dipole moment:

$$\Omega_R = \frac{d_{eg}^* E_0}{\hbar} . \tag{2.3.19}$$

It is well known from the atomic physics that the strong laser field causes the dynamic Stark splitting of the atomic levels [4]. The energy separation of these features is predicted to be described by equation (2.3.20). Since for the resonant case it is directly related to the Rabi frequency

$$E_{Rabi} = \hbar\Omega_R = d_{eg}^* E_0 \tag{2.3.20}$$

Taking into account the relation (2.3.21) between transition dipole moment and oscillator strength f

$$|d_{eg}|^2 = \frac{\hbar e^2}{2m_e\omega_{eg}} f\,, \tag{2.3.21}$$

one can get the energy gap dependence on the transition oscillator strength

$$E_{Rabi} = E_0\sqrt{\frac{\hbar e^2}{2m_e\omega_{eg}} f}\,, \tag{2.3.22}$$

where m_e is electron mass.

Experiments performed to study exciton and photon interaction phenomena in a quantum microcavity revealed that strong coupling manifests itself as formation of separated minima on the reflectance curve. The energy difference between the minima is linearly dependent on the square root of the oscillator strength of the cavity mode [1]. The same kind of behavior was recently shown for SPP/exciton coupling [8].

In general case quantum Jaynes – Cummings model predicts that Rabi frequency is dependent on amount of photons interacting with two level system. So the energy separation should become intensity dependent. Only in the case of the vacuum Rabi splitting mentioned above the intensity is independent on intensity, because only one photon in a time interacts with two level system.

2.4. Coupled oscillators model

In order to describe SPPs interaction with absorbing medium also a coupled oscillator's model can be used. The classical and quantum mechanical treatment of coupled oscillator's problem predicts very similar behavior of the system.

Consider the multilayer structure that consists of a silver layer and a dielectric absorbing medium. The dielectric medium is formed by a non-absorbing matrix material and absorbing molecules that are embedded in the matrix. Assume that the molecule has one allowed optical transition, so that an exciton with energy E_{Ex} and linewidth γ_{Ex} can be associated with the molecule. SPPs can be excited in such structure by one of the techniques described in section 3.1. The set of equations describing the SPP interaction with the exciton can be written as

$$\begin{pmatrix} E_{SPP}(\mathrm{Re}[k_x]) - i\gamma_{SPP} & V \\ V & E_{Ex} - i\gamma_{Ex} \end{pmatrix} \begin{pmatrix} x_1 \\ x_2 \end{pmatrix} = \varepsilon \begin{pmatrix} x_1 \\ x_2 \end{pmatrix}, \tag{2.3.1}$$

where $E_{SPP}(\mathrm{Re}[k_x])$ is an energy of the uncoupled SPP at the interface between the silver layer and the dielectric matrix (without absorbing molecules), γ_{SPP} is a linewidths of SPP. It is assumed that the linewidth is independent on the wave vector. Parameter V is a coupling strength between the SPP and the exciton. This parameter is usually varied in order to get good agreement with experimental dispersion data. Parameter ε is energy of the coupled state. If the system of linear equations has non-trivial solution, the determinant of the system must be equal to zero. It is easy to write such equation for the system (2.3.1). The equation has two solutions, which describe two branches of the SPP's dispersion curve. Note that the solutions are complex. The complex energy describes exponential damping of oscillations. At resonant conditions, when $E_{SPP}(\mathrm{Re}[k_{x,resonant}]) = E_{Ex}$, the difference between upper and lower branch energy values is named an energy gap value ΔE. It is easily calculated from (2.3.1)

$$\Delta E = \sqrt{4V^2 - (\gamma_{SPP} - \gamma_{Ex})^2}\ . \tag{2.3.2}$$

Very often the broadening of the electronic transition as well as the SPP linewidth are neglected and the energy gap value becomes simply

$$\Delta E = 2V\ . \tag{2.3.3}$$

The presence of the damping terms results in the decrease of the energy gap according to (2.3.2).

One can compare the equation (2.3.3) to the equation (1.1) and get that

$$V \propto \sqrt{f_{ex}}\ , \tag{2.3.4}$$

where f_{ex} is the exciton oscillator strength per unite area. It will be shown later (section 4.3) that f_{ex} depends on the absorbing molecule concentration. So, changing the dye molecule

concentration could change the energy gap value. The equation (2.3.2) reveals other way to change the energy gap. The SPP linewidth γ_{SPP} is inversely proportional to the SPP lifetime. So, the decrease (increase) of the SPP lifetime leads to the increase (decrease) of the energy gap value.

The similar reasoning holds for the SPP coupling to dye molecules, which possess two absorption maxima. Now two excitons E_{Ex1} and E_{Ex2} are associated with the resonant absorber. The system of the equations that describes SPP interaction with two excitons is

$$\begin{pmatrix} E_{SPP}(k_x) - i\gamma_{SPP} & V_1 & V_2 \\ V_1 & E_{Ex1} - i\gamma_{Ex1} & 0 \\ V_2 & 0 & E_{Ex2} - i\gamma_{Ex2} \end{pmatrix} \begin{pmatrix} x_1 \\ x_2 \\ x_3 \end{pmatrix} = \varepsilon \begin{pmatrix} x_1 \\ x_2 \\ x_3 \end{pmatrix} \tag{2.3.5}$$

$$\text{or} \begin{pmatrix} E_{SPP}(\mathrm{Re}[k_x]) & V_1 & V_2 \\ V_1 & E_{Ex1} & 0 \\ V_2 & 0 & E_{Ex2} \end{pmatrix} \begin{pmatrix} x_1 \\ x_2 \\ x_3 \end{pmatrix} = \varepsilon \begin{pmatrix} x_1 \\ x_2 \\ x_3 \end{pmatrix}. \tag{2.3.6}$$

Here γ_{Ex1} and γ_{Ex2} are linewidths of excitons; V_1 and V_2 .are the coupling strengths to two excitons. The remaining task is to solve the equation (2.3.5) for the energy of the coupled state as a function of *x*-component of the wave vector:

$$(E_{SPP}(\mathrm{Re}[k_x]) - i\gamma_{SPP} - \varepsilon)(E_{Ex1} - i\gamma_{Ex1} - \varepsilon)(E_{Ex2} - i\gamma_{Ex2} - \varepsilon) - (E_{Ex1} - i\gamma_{Ex1} - \varepsilon)V_2^2 - (E_{Ex2} - i\gamma_{Ex2} - \varepsilon)V_1^2 = 0 \tag{2.3.7a}$$

$$\text{or } (E_{SPP}(\mathrm{Re}[k_x]) - \varepsilon)(E_{Ex1} - \varepsilon)(E_{Ex2} - \varepsilon) - (E_{Ex1} - \varepsilon)V_2^2 - (E_{Ex2} - \varepsilon)V_1^2 = 0, \tag{2.3.7b}$$

when the damping terms are neglected.

In this thesis the solutions of the equation (2.3.7b) are used to fit the experimental dispersion relations. But one should always keep in mind the approximation and be careful in the data comparison. To illustrate this let us consider an example. Equations (2.3.7a) and (2.3.7b) have solutions, which in general case are complex functions of E_{Ex1}, E_{Ex2}, V_1 and V_2. At the resonant condition, when for example $E_{SPP}(\mathrm{Re}[k_{x,resonant}]) = E_{Ex1}$, the difference between the upper and the middle branch values is named an upper energy gap value ΔE_U (it is assumed that $E_{Ex1} > E_{Ex2}$). When $E_{SPP}(\mathrm{Re}[k_x]) = E_{Ex2}$, the difference between the middle and the lower branch values is named a lower energy gap value ΔE_L. Consider the upper energy gap value ΔE_U as a function of the SPP linewidth γ_{SPP} (figure 2.3.1). For doing this let us consider

Sulforhodamine 101 molecules embedded into SU-8 dielectric matrix. For this absorbing medium the exciton energies are $E_{Ex1} = 2.23$ eV, and $E_{Ex2} = 2.07$ eV; the linewidths of excitons are $\gamma_{Ex1} = 0.15$ eV and $\gamma_{Ex2} = 0.14$ eV (these values are obtained from Sulforhodamine 101 solutions absorption measurements). Values of V_1 and V_2 are taken from the table B.2 that can be found in the appendix B. These values are parameters used to fit experimentally obtained dispersion relations of samples with different Sulforhodamine 101 concentrations. One can see in figure 2.3.1 that the upper energy gap value does not decrease monotonously with increasing SPP linewidth as it is predicted for the single exciton system, but it has more complex behavior.

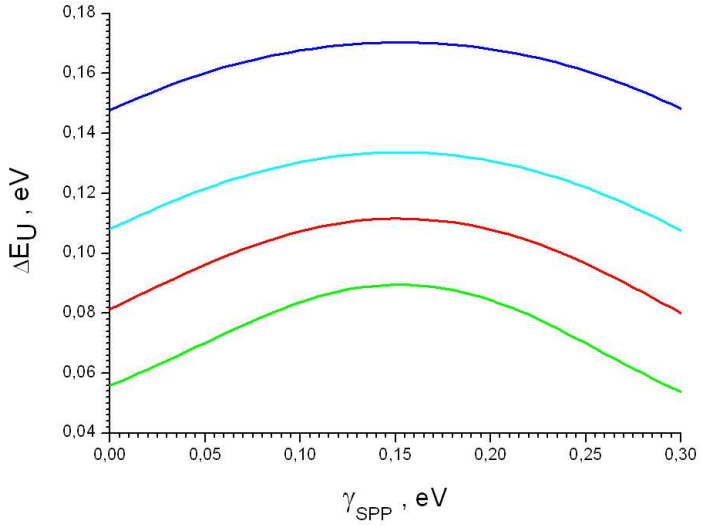

Figure 2.3.1 Upper energy gap as a function of the SPP linewidth. Blue curve corresponds to the case, when V_1 = 0.17 eV, V_2 = 0.075 eV; cyan curve – V_1 = 0.15 eV, V_2 = 0.06 eV; red curve – V_1 = 0.13 eV, V_2 = 0.05 eV; green curve – V_1 = 0.11 eV, V_2 = 0.04 eV.

3. Experimental techniques in surface plasmon polaritons study

3.1. Surface plasmon polaritons excitation methods

A straightforward method to excite SPPs at a metal/vacuum interface is illumination of the metal layer with *p*-polarized light. But special arrangements must be introduced to get coupling. The dispersion relation, as a function of the wave vector component parallel to the interface, k_x, for the light in vacuum that incident to the surface at an angle θ is

$$k_{x,light} = \frac{\omega}{c}\sin\theta . \qquad (3.1.1)$$

It was shown in chapter 2.1 that the dispersion relation for SPPs propagating at metal/dielectric interface is (2.1.16)

$$k_{x,SPP} = \frac{\omega}{c}\sqrt{\frac{\varepsilon_1\varepsilon_2}{\varepsilon_1+\varepsilon_2}} ,$$

where ε_1 is dielectric permittivity of the insulator and ε_2 is dielectric permittivity of the metal.

Figure 3.1.1 shows dispersion relations of light propagating in vacuum and SPPs for silver/Sulforhodamine 101 resin interface (semi-infinite layers). To excite SPP the component of the wave vector of the incident light parallel to the surface ($k_{x,light}$) must be equal to the SPP wave vector component parallel to the surface ($k_{x,SPP}$). In figure 3.1.1 one can see that SPP wave vector component is larger than light wave vector component. To provide matching conditions or to make

$$k_{x,light} + \Delta k_x = k_{SPP,x} \qquad (3.1.2)$$

one can introduce an additional dielectric layer ($\varepsilon > 1$). The dispersion relation of the light in a dielectric media is

$$k_{x,light} = \frac{\omega\sqrt{\varepsilon}}{c}\sin\theta \qquad (3.1.3)$$

From figure 3.1.1 one can see that after introducing additional dielectric layer the coupling is possible. By varying the angle of incidence one can couple the light to every point of the SPP dispersion curve.

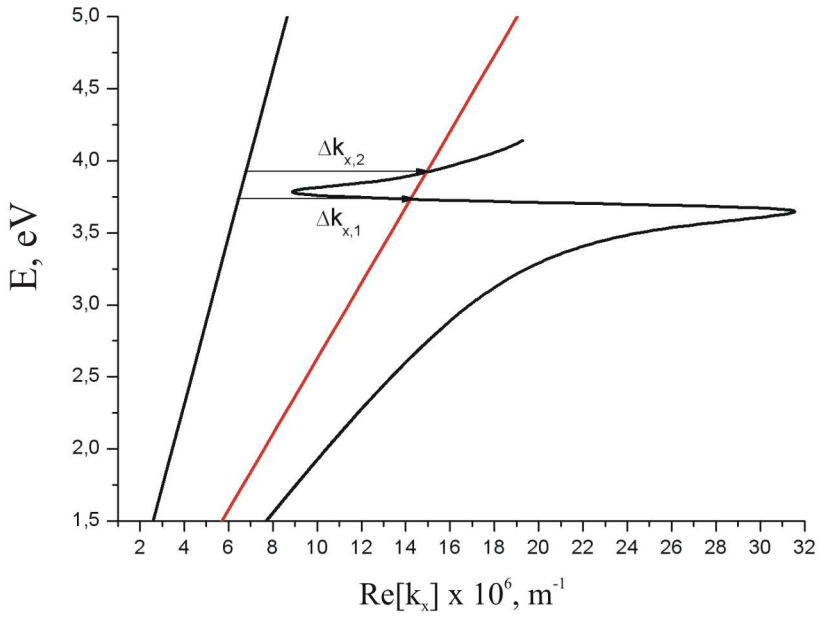

Figure 3.1.1 SPPs dispersion relation for silver (50 nm)/ Sulforhodamine101 resin (50 nm) structure, dispersion relations of light propagating in vacuum (black line) and dispersion relations of light propagating in media with $\varepsilon = 1.5^2$ (red line). The arrows indicate the change in wave vector component parallel to interface due to the additional dielectric layer. The angle of incidence is 40º in both cases.

The most common optical excitation technique is based on the prism coupling. In a so-called Kretschmann configuration (figure 3.1.2 (a)) the metal film (or multilayered structure) is illuminated through a dielectric prism at an angle of incidence greater than the critical angle for total internal reflection. If the frequency and wavevector-matching requirement are fulfilled, light tunnels through the metal film (the thickness of the film must be thin, *e.g.* 50nm for optical radiation) and excites SPP at the external metal interface. As a result of the SPP excitement one observes minima in the detected reflectivity [27].

If one introduces an additional thin dielectric layer between the prism and the metal layer, SPPs can be excited at internal metal interface as well (figure 3.1.2 b). Then varying the angle of incidence one can fulfill the matching conditions for the internal interface. So the SPP excitation can occur at both interfaces [27].

In Otto configuration (figure 3.1.2 c) the gap between the prism and the metal layer is introduced. The total internal reflection occurs at the prism/air interface, the decaying wave travels through the gap and excites SPP at air/metal interface. Such arrangement provides necessary matching conditions to excite SPPs at thick metallic layers.

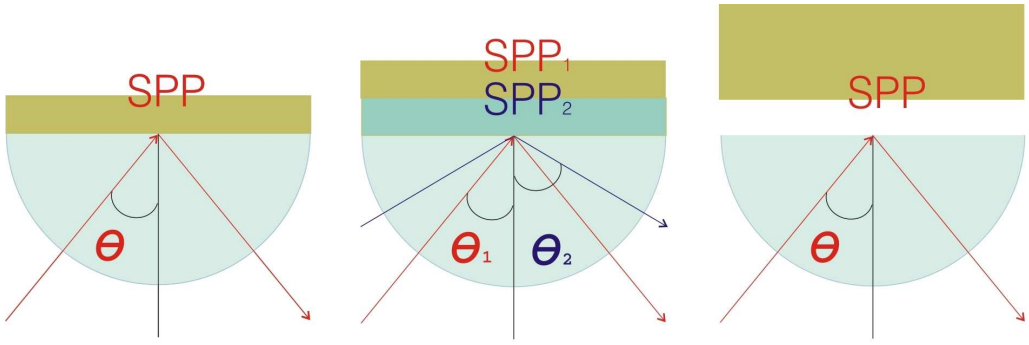

Figure 3.1.2 SPP optical excitation configurations. a) Kretschmann configuration; b) Kretschmann configuration with an additional dielectric layer; c) Otto configuration.

An alternative excitation method that can be used is a coupling with help of a microscope objective with high numerical aperture. An oil-emersion objective is in contact with the glass substrate (the metal layer is on the top of the substrate). The high numerical amplitude provides an angular spread (the angles greater than critical angle of total internal refraction are present) of focused excitation light, so the total internal reflection occurs at glass/air interface [21].

Diffraction effects can be also be used to fulfill the equation (3.1.2). The diffraction grating can be created on a certain place of the smooth metallic film. Consider a planar periodic structure with period d (in both directions) that is placed in media with ε_m. As a result of the interaction of incident *p*-polarized light with the periodic structure a change in the wave vector occurs. SPPs will be excited if the matching condition holds

$$\vec{k}_{SPP} = \vec{e}_{SPP}\frac{\omega\sqrt{\varepsilon_m}}{c}\sin\theta \pm p\frac{2\pi}{d}\vec{a} \pm q\frac{2\pi}{d}\vec{b}\,, \qquad (3.1.4)$$

where $\vec{e}_{SPP}$ is the unit vector in the direction of in-plane component of the incident light, $\vec{a}$ and $\vec{b}$ are the unit lattice vectors of the structure and p, q are integer numbers. By varying the grating parameters and film thickness, SPPs can be excited on both interfaces of the metal layer [21].

Randomly rough surface can provide matching condition (3.1.4) without any special arrangement, because in the near-field region of the diffracted light all wave vectors are present [27]. But the efficiency of coupling in the case of rough surface is very low.

The very neat method to excite SPP is the excitation with SNOM (scanning near-field microscopy). A small probe tip illuminates the metal surface in the near-field, so the radiation of any wavevectors is present at the interface. The SPPs can thus be excited locally and at any place of the metal film.

The brilliant coupling method was used recently by *Hakala et al.* [17]. Organic dye molecules can be used as couplers between far-field light and near-field light. The method has several advantages: no special geometry is required; any light source can be used. The dye molecules (Coumarin 30 was used as a donor, Rhodamine 6G was used as an acceptor,) are imbedded into SU-8 polymer resin. The positioning of the molecules was done by e-beam lithography. Before positioning the molecules 50 μm long silver waveguide was fabricated on top of the ITO coated glass. The excitation of the donor molecule was done by 405 nm diode laser. At the same time a confocal microscope scanner collected the light from the whole sample. It was shown that SPPs excited by the Coumarin 30 fluorescence can propagate even ~10 μm, then excite the acceptor molecules and finally the Rhodamine 6G fluorescence was detected in far-field.

This kind of excitation method can be combined with the conventional Kretschmann geometry experimental techniques. For this purpose the excited fluorescent molecule is placed in a vicinity of the metallic film. The excited fluorescent molecule can then decay non-radiatively into SPPs modes. The SPPs then being scattered on metallic film imperfections radiate into the glass substrate and employing the prism the scattered light can be detected at certain angles. This method is called reverse Kretschmann method [28].

3.2. Surface plasmon polaritons detection methods

The successful excitation of SPPs by prism or grating coupling techniques can be easily deduced from a decrease in the intensity of reflected beam. When direct visualization of propagating SPPs is desirable one can use on of the following methods: SNOM (SNOM in collecting light mode – photon scanning tunneling microscopy), imaging based on fluorescence [17, 29], scattered light collection, *etc*.

Photon scanning tunneling microscopy The small probe tip is brought into vicinity (within a distance l_{skin2} (see the equation (2.1.18))) of the surface of the structure. The evanescent light in the near-field that is collected by the tip (the metalized etched end of an optical fiber with a small aperture) is converted to propagating modes in the optical fiber. The resolution is limited by the size of the fiber aperture.

Fluorescent imaging is based on collection of the radiation emitted by fluorescent molecules or quantum dots that are placed on the metal surface (within the evanescent SPP field). These emitters usually have broad absorption band. If the frequency of propagating SPPs lies within the band the excitation of emitters is possible. The intensity of the emitted radiation is proportional to the intensity of SPPs field at the emitter position. If one places a thin spacer between metal and the layer of fluorescent molecules the enhancement of fluorescence can be achieved, because the non-radiative quenching of the fluorescence does not occur.

Scattered light collection The propagation of SPPs at air/metal interface can be imaged by collecting the light that is scattered at film imperfections. This method cannot be used for films with excellent surface quality. The neat experiment based on this technique was performed by *Depine et al* [21]. The metal surface was corrugated with a blazed grating, the excitation was done by He-Ne laser and the scattered light was projected to the screen parallel to the structure. Using such setup makes possible the determination of the band gaps of SPPs for films with blazed grating.

4. Experimental study of three layers structures

4.1. Sample fabrication techniques

The schematic structure of the studied samples is shown on figure 4.1.1. The sample is fabricated on top of a cover glass with dimensions of 15 mm × 15 mm, thickness ≈ 0.15 mm, purchased from *Knittel Gläser*. The glasses are used after advanced cleaning procedures. First, glasses are cleaned with hot acetone, and then while being into hot isopropanol alcohol glasses are cleaned by ultrasound (*2-5* minutes). After that glass is dried in dry nitrogen flow. Next the silver layer is formed on top of the glass substrate by electron-beam evaporation in an ultra-high vacuum (10^{-9}-10^{-8} mbar). The typical thickness of the metal layer is 55 nm. It was verified with AFM (atomic force microscopy). It should be noticed that metallic film is semi-continuous. At first, metallic grains are formed on the glass substrate, as evaporation continues coalescence occurs and clusters are formed. At the percolation threshold insulator-metal transition takes place, the voids become smaller and irregular. Finally, the metal filling factor increases, so the film could be considered as metallic. The size of the clusters is dependent on evaporation rate (figure 4.1.2). The higher filling factor was achieved for films evaporated at higher rates. There is contradicting information in literature about the evaporation rates of Ag layers for optical studies. In [23] 5 nm/s rate was used to get smooth surfaces, but further polishing was required. In [25] 0.05 nm/s rate was chosen to obtain lower roughness (1.7-2.9 RMS). At present work the low evaporation rate is chosen 0.02-0.04 nm/s to get smoother surfaces and reduce formation of Ag clusters with the characteristic size of μm (the example of the clusters is shown in figure 4.1.3). It was noticed that the higher the rate of the silver evaporation the more clusters formed on the surface.

Figure 4.1.1 Schematic structure of the samples.

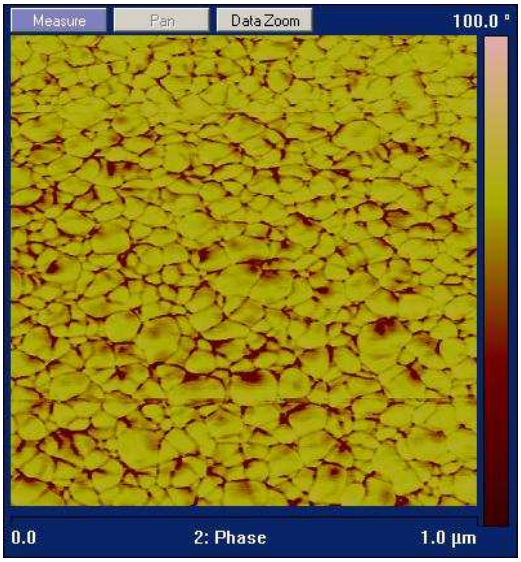

a)

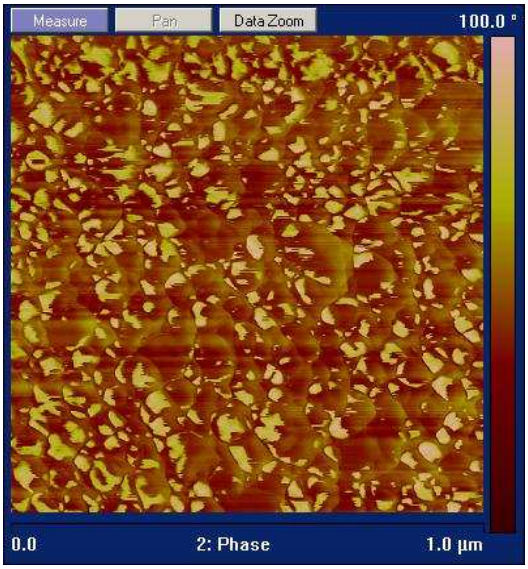

b)

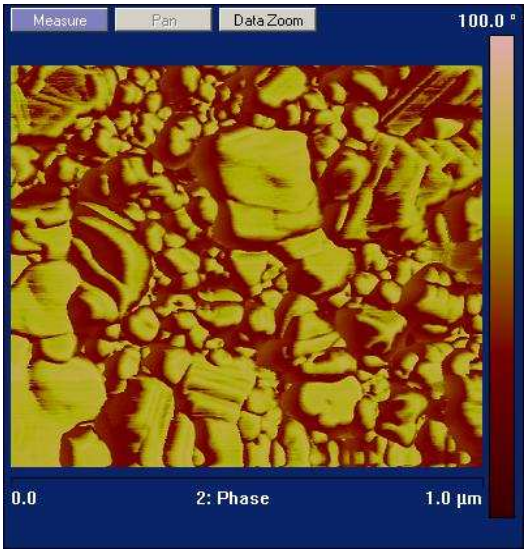

c)

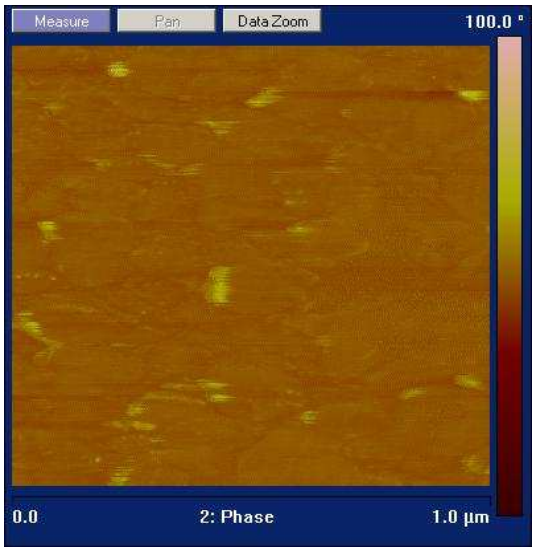

d)

Figure 4.1.2 AFM phase images of the semi-continuous silver films fabricated at different evaporation rates: a) 0.04 nm/s; b) 0.29 nm/s; c) 0.7 nm/s; d) 1.98 nm/s.

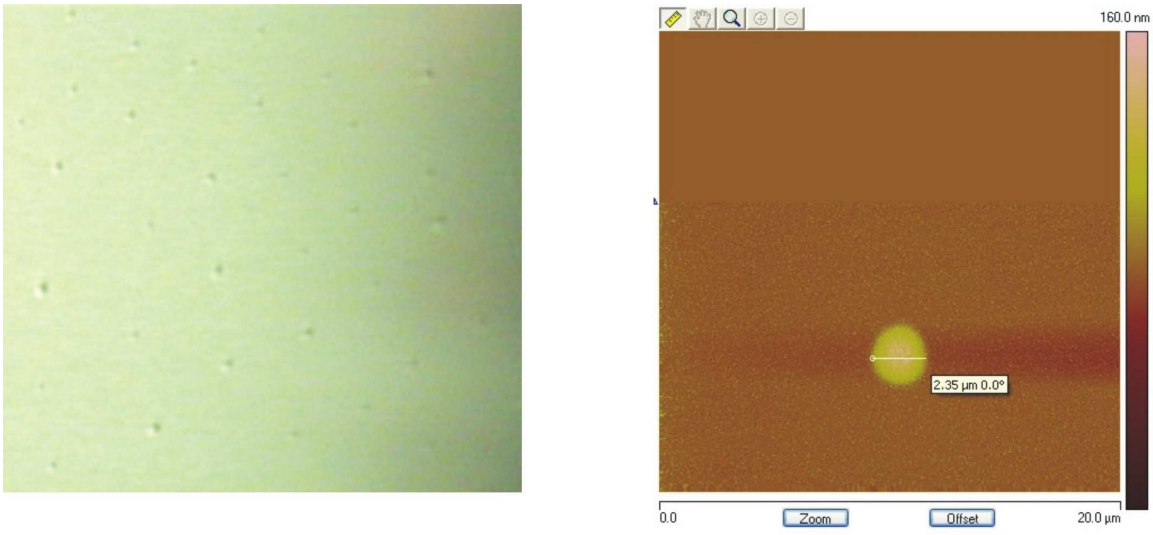

Figure 4.1.3 a) optical image of µm Ag clusters formed during thin film deposition by electron beam evaporation with rate 0.34 nm/s; b) AFM image of a cluster.

On top of the metal film the resist that contains the desirable organic molecules was spun. In this work six samples with different Sulforhodamine 101 concentrations were prepared. SU-8 epoxy-based negative polymer resist was used as matrix. In order to get desirable thickness of the resist layer commercially available Microchem SU-8 2025 was dissolved with cyclopentanone in volume ratio *1:6*. Using this root solution one can get layer thickness of 800 nm when rotational speed is 5000 rpm. To get thinner layers the SU-8 should be dissolved more. The appropriate solvent for Sulforhodamine 101 is ethanol alcohol. But it is also known that SU-8 has a tendency to make aggregates (irregular shaped particles and fibers) in ethanol [30]. So one should chose amounts of SU-8 and ethanol carefully in order to prevent the aggregation. The typical recipe of the resist is following. Desirable amount (1-5 mg) of Sulforhodamine 101 (purchased from Sigma Aldrich) were dissolved in 300 µl ethanol. To this solution 4.5 ml cyclopentanone mixed with 420 µl SU-8 root solution was added. It was noticed that in solutions that contained more than 3 mg Sulforhodamine 101 a colloidal solution was formed due to the lack of ethanol. Further filtering was used to remove aggregates with size above *0.2* µm.

After the filtration the resist is spun on top of the silver (or chemically cleaned glass for reference samples) and sample is baked at 95ºC to evaporate the solvent and polymerize

the resin. To get resist thickness ≈ 50 nm the spinning rate was chosen to be 4500 rpm. The thickness of the resist layer was verified with AFM. It should be mentioned that the resist film is not totally smooth. The profile of the film shows presence of aggregates (20-50 nm) possibly due to SU-8 photoresist aggregation in ethanol or Sulforhodamine 101 aggregates formation.

For absorption measurement reference samples without silver were fabricated. The absorbance spectra were measured with Perkin Elmer UV/VIS Lambda 850 spectrometer. The absorbance curves are shown in figure 4.1.4. The absorbance spectra were fitted with two lorentzian curves and the absorbance maxima were determined to be around 555 nm (2.07 eV) and 599 nm (2.23 eV). The wavelengths of the maxima do not change significantly for the samples under study.

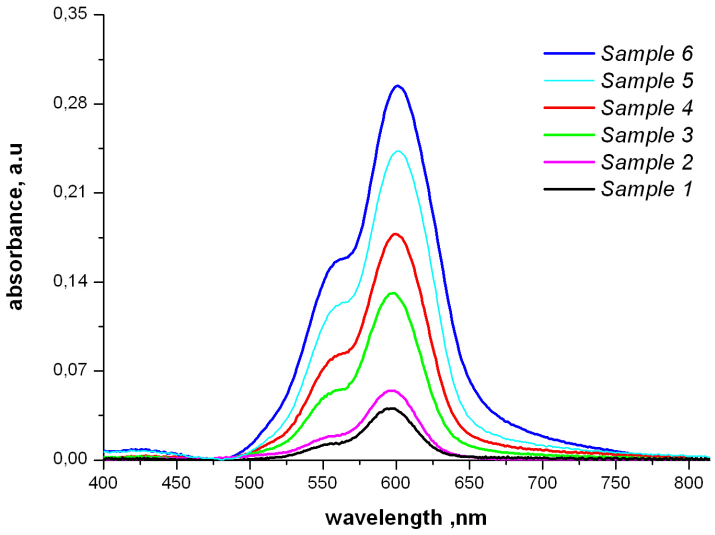

Figure 4.1.4 Absorbance of Sulforhodamine101 resin layer spun on top of the glass substrate. The Sulforhodamine 101 concentration increases from sample 1 to sample 6.

Also a sample having Ag layer (50 nm) and SU-8 resin layer (50 nm) without dye molecule was prepared. It was used to study the SPP dispersion relation at silver/SU8 layer interface.

4.2. Coupling method and experimental setup

The figure 4.2.1 shows the schematic picture of the experimental setup. The hemicylindrical prism made of BK7 glass in Kretschmann configuration is used. The prism average index of refraction for optical range is calculated to be *1.52*. To get continuous index of refraction between the prism glass and the glass substrate index matching oil with the same refractive index was used. For excitation Oriel *66182* white light source is used. The spectral characteristic of the white light source is shown on figure 4.2.2. In the analysis of the reflectometry data the collected light intensity is divided by incident light intensity, so the shape of spectral profile does not affect the wavelength data.

The light is collimated and aligned by using two slits. Rotatable Glan Taylor prism polarizer is used to adjust the polarization of the light. The incident angle of the incoming light is adjusted manually by a goniometric prism mount.

In the experiment one can obtain the wave vector component parallel to the interface, k_x

$$k_{x,light} = \frac{\omega\sqrt{\varepsilon_{prism}}}{c}\sin\theta, \qquad (4.1.1)$$

where ω is the excitation frequency, ε_{prism} is dielectric permittivity of the prism material (the dispersion of BK7 glass is neglected) and θ is the angle between the normal to the sample surface and the normal to the wave front , e.g. the angle of incidence. The angle of incidence can be read from the scale of the rotating mount. To measure the frequency of light that excites SPPs the reflected (detection 1) and transmitted (detection 2) light spectra are collected by an optic fiber connected Jobin Yvon *iHR320* spectrometer equipped with Jobin Yvon Symphony CCD camera.

The methods of the excitation and detection are simple to perform, but they have some disadvantages. According to section 3.1 and figure 3.1.1 in this coupling method (fixed angle of incidence and changing wavelength) the light line “cuts” the SPP dispersion curve of the multilayer sample under present study in a way that more than one cross is possible. Thus, in the reflected spectrum one observes more than one dip. So, one has to think about the resolution of the detection because due to big FWHM the dips can overlap.

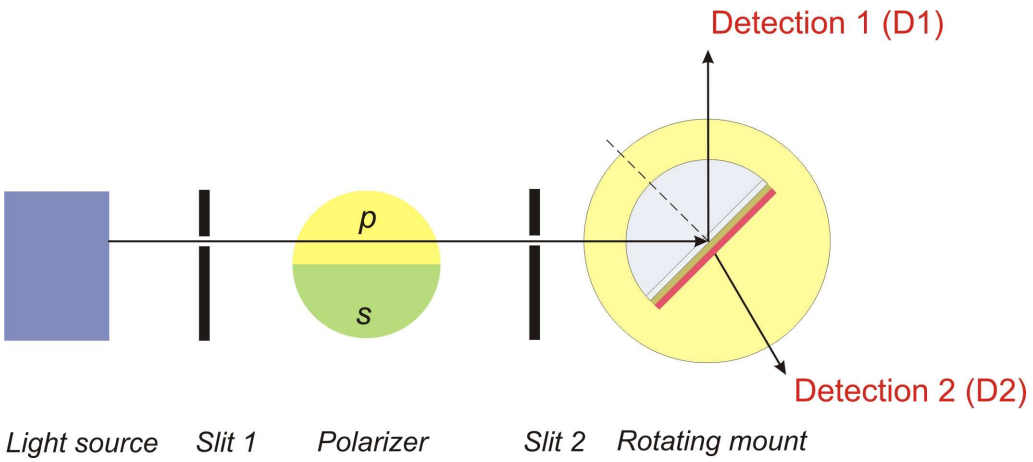

Figure 4.2.1 Schematic representation of the experimental setup.

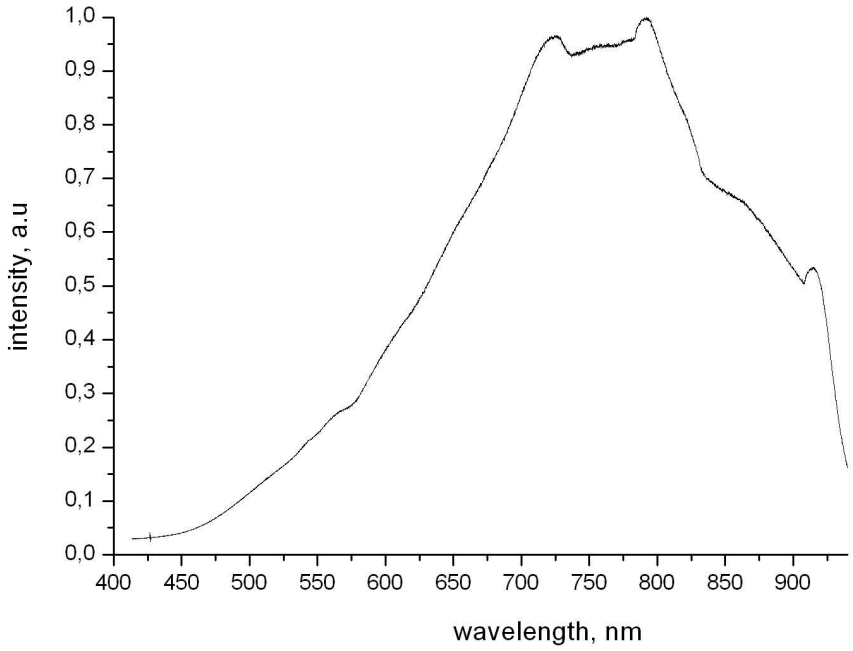

Figure 4.2.2 The spectrum of Oriel *66182* white light source. The water filter is placed between the lamp and the detector. The filament current is 10.5 A, the applied voltage is 20 V. The spectrum is normalized.

4.3. Dispersion curves of surface plasmon polaritons propagating in three layers structures

The dispersion relation is a fundamental property of SPP. In this chapter the dispersion relations obtained experimentally for samples with different Sulforhodamine 101 concentrations are considered. The dispersion curves can be achieved performing reflectometry measurements (D1 in the figure 4.2.1) or detecting the radiation resulting from SPPs scattering to photons (D2 in the figure 4.2.1). The reflectometry measurements were done using the setup described in previous section. The angles were read from the scale of the goniometric tool, the coupled wavelengths were obtained from fitting of the dips in the reflectance curve with lorentzian curves. Then the dispersion curves $\mathrm{E} = \mathrm{E}(\mathrm{Re}[k_x])$ were built.

As it was discussed in section 2.1, in general case the wave vector is treated as complex value $k_x = \mathrm{Re}[k_x] + i\,\mathrm{Im}[k_x]$. Figure 4.3.1 represents dependences $\mathrm{E} = \mathrm{E}(\mathrm{Re}[k_x])$ and $\mathrm{E} = \mathrm{E}(\mathrm{Im}[k_x])$ for semi-infinite silver and semi-infinite Sulforhodamine 101 resin structure calculated using (2.1.16) and (2.2.13). As it can be seen from figure $\mathrm{Re}[k_x] \approx 3\,\mathrm{Im}[k_x]$ in the strong coupling region, so one cannot totally neglect imaginary part of k_x. In such situation the appropriate parameters to present the experimental data could be the wavelength of surface plasmon resonance as a function of angle, as it was done in [31]. But nowadays the most authors present the result in the form of the SPPs dispersion curves $E = E(k_x) \approx E(\mathrm{Re}[k_x])$. This is justified since the real part of the in-plane wave vector component describes the SPP propagation, while the imaginary part describes its dissipation, which does not need to be considered while discussing pure dispersion properties. In this study the representation of the dispersion relation is $E = E(\mathrm{Re}[k_x])$.

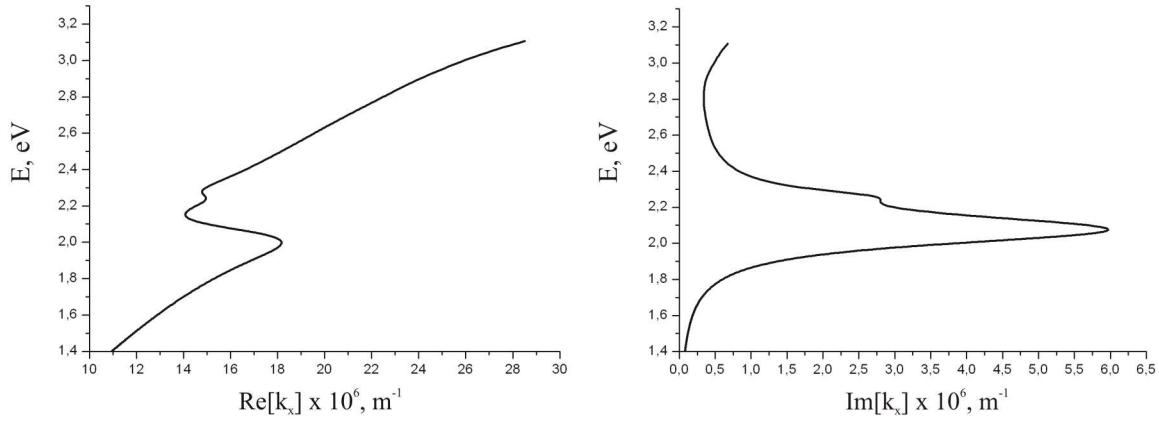

a) b)

Figure 4.3.1 a) Energy of SSPs as a function of $\mathrm{Re}[k_x]$, b) energy of SSPs as a function of $\mathrm{Im}[k_x]$. The calculations were done for semi-infinite Silver and semi-infinite Sulforhodamine 101 resin structure.

First, the sample without Sulforhodamine 101 molecule layer was studied. 55 nm of silver were evaporated on the top of glass substrate. An example of measured reflected light spectrum is shown in the figure 4.3.2. Also theoretically calculated curves for the reflectance of such a structure are shown. To obtain theoretical curves the transition matrix method (section 2.2) was used. The theoretical and experimental data do not overlap perfectly. There are several reasons for the discrepancy. The first reason is related to the silver film preparation difference, i.e., *Christie* and *Johnson* [23] used 34 nm films evaporated with high rate (about 5 nm/s), after what films were polished. In opposition the films used in this project are evaporated with very low speed about 0.04 nm/s and thickness of the films is about 55 nm. No special treatment was done after the metal evaporation. Examination of the films with AFM shows (figure 4.1.2) that the film surface is quite rough. It was shown by *V.P. Drachev et al.* that the surface roughness could affect the metal dielectric function (imaginary part) [25]. The authors concluded that chemical interface effects (grain boundary has different properties from the grain bulk) and defects in the film have critical influence on the silver dielectric function. The other reasons are that the prism material dispersion is not taken into account in the calculations as well as the presence of the glass substrate and the index matching oil.

As one can see, the reflectance curve calculated with silver dielectric permittivity from [23] is in better agreement with presented experimental data. So for all calculations in this thesis the silver dielectric function from [23] was used.

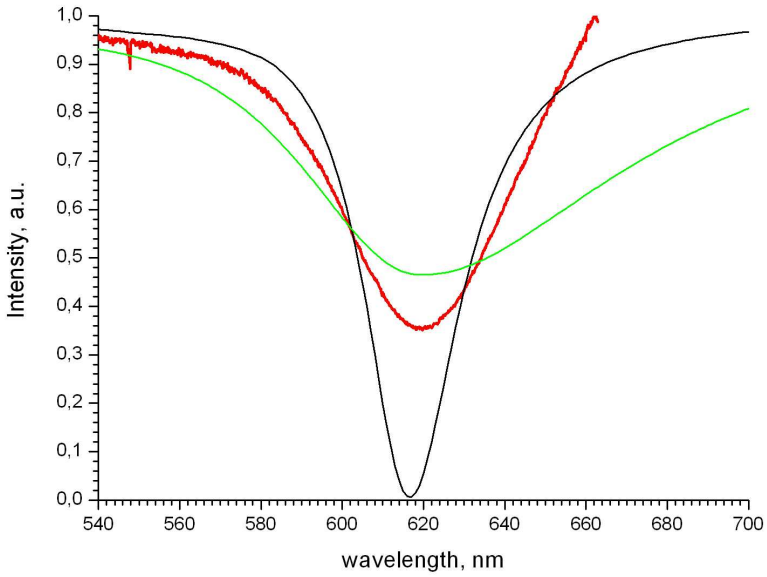

Figure 4.3.2 Intensity of the reflected light measured at detection position D1 for 55 nm silver layer divided by incident light spectrum (red curve). Angle of light incidence is 42º 30'. The theoretical reflectance curves for the same structure and the same angle of incidence using dielectric permittivity for silver from [23] (black curve) and [31] (green curve) are plotted. Experimental and theoretical data were normalized.

The second set of refractometry measurements was done for six samples that contain Sulforhodamine 101 molecule in different concentrations. The absorption curves of the test samples are shown in section 4.1 in the figure 4.1.4. Examples the measured reflectance spectra divided by the incident light intensity together with calculated ones are shown on figure 4.3.3. Later we will discuss the details of the calculations. It should be noted that the use of the name “reflectance coefficient” for the experimental curve is not quite valid. The definition of reflectance coefficient was done in the section 2.2 (2.2.12) and the calculation was done according to the definition. Reflectance coefficient is the relation of average energy flux density of reflected light to the average energy flux density of incident light measured at the same point in space. But the measurement cannot be performed according to the definition. The result is

dependent on the detector position while collecting incident and reflected radiation. In this work the reflected light spectrum was divided by incident light spectrum and then the result was normalized. This notation is related to the absolute values of reflectance coefficient, but the wavelength dependence of the refraction coefficient cannot be changed. There is another fact that affects the wavelength dependence — the non-linear intensity dependence of the CCD response. The square-root response function was used, but in reality it is more complex dependence. The tilt of the experimental reflectance curve is probably due to this discrepancy. The careful calibration of the device should be done to properly perform the reflection coefficient analysis. Thus, one can conclude that quantitative comparison of theoretical and experimental reflectance coefficient values is not possible in this work. But still the frequency of the reflectance minima can be determined within a reasonable error interval.

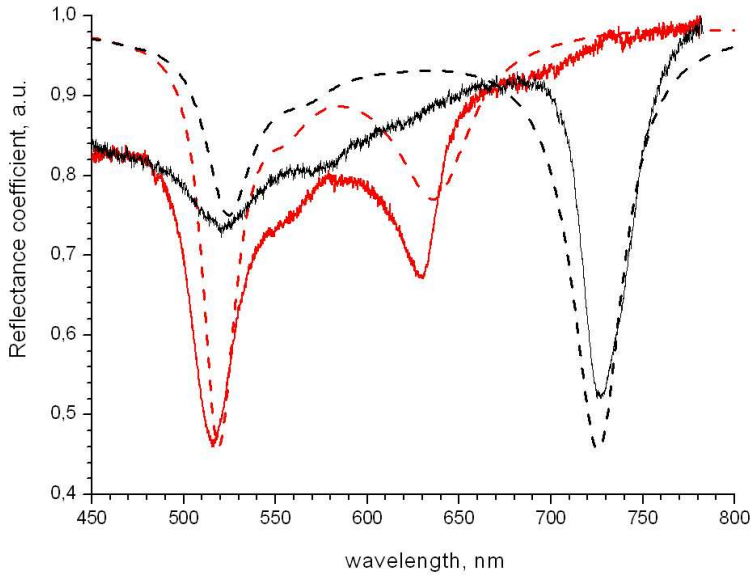

Figure 4.3.3 Experimentally obtained reflection coefficient curves (red curve for sample 3 and black curve for sample 6) and theoretically predicted reflection coefficients (red dashed curve for sample 3 and black dashed curve for sample 6) as a function of light wavelength. The angle of incidence is 75º.

In the figure 4.3.4 the wavelength dependence of the observed minima on the angle of incidence is shown. For convenience instead of angle of incidence θ we use angle $(90^\circ - \theta)$. Also this figure represents density plots of calculated reflectance coefficient using transfer matrix method for six samples under study as a function of light wavelength and angle.

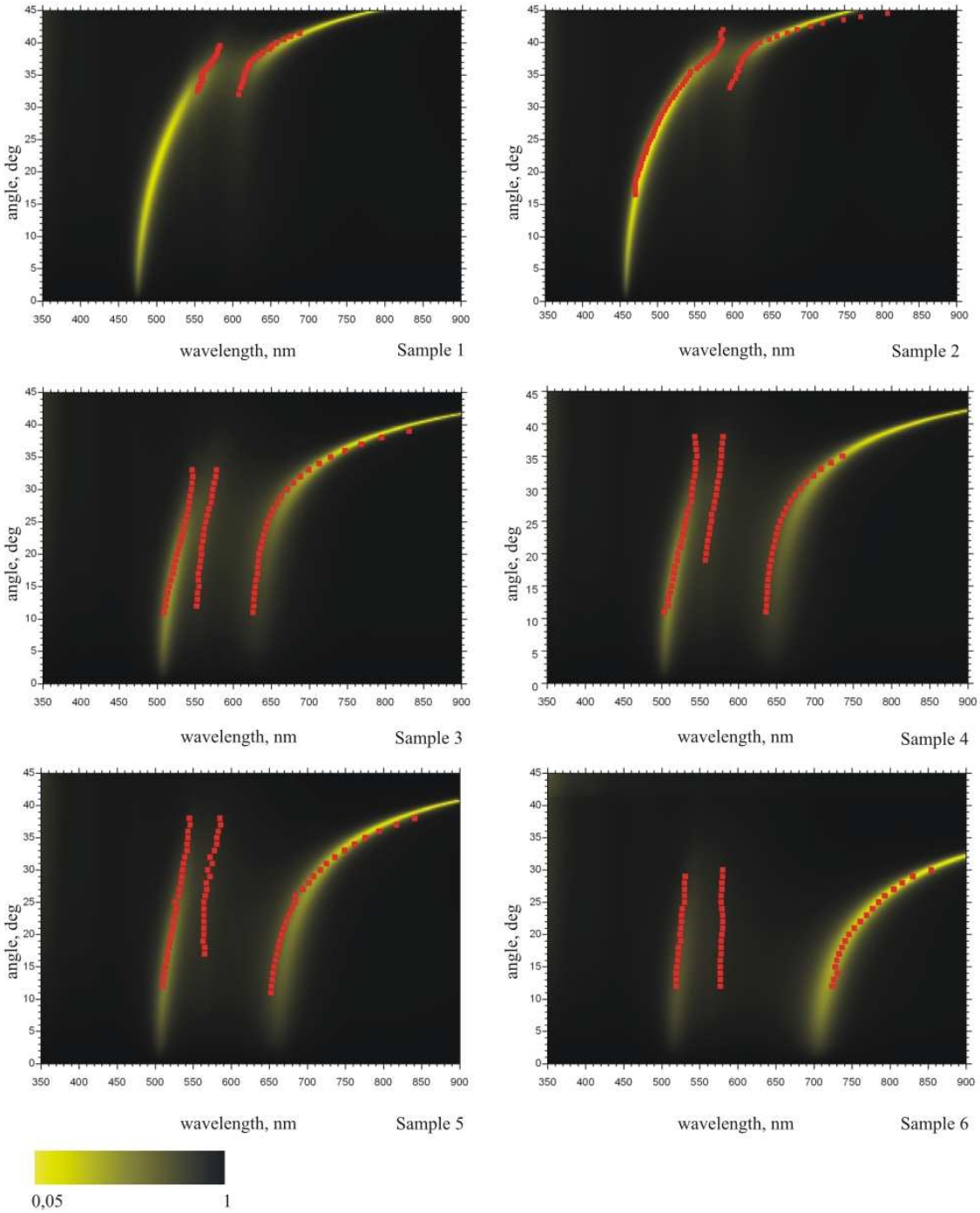

Figure 4.3.4 Calculated reflectance coefficients as a function of wavelength and angle for six samples under study. Color represents the value of reflectance coefficient. Experimentally obtained wavelength dependences of the observed reflectance spectrum minima is represented as red dots as a function of the angle of incidence.

As was discussed at the section 2.2, to calculate the reflection coefficient of a multilayer sample it is necessary to know the dielectric functions of every layer. The choice of silver dielectric function was discussed above. The dielectric function of Sulforhodamine 101 layer can be described by (2.2.13) that is based on the oscillator model of molecular dispersion

$$\varepsilon(\omega) = \varepsilon_S + \sum_{i=1}^{2} \frac{A_i \omega_{0i}^2}{\omega_{0i}^2 - \omega^2 - i\omega\gamma_i}, \qquad (4.3.1)$$

where ε_S is a frequency independent dielectric permittivity of the media that is hosting the Sulforhodamine 101 molecule; A_i is dimensionless parameter characterizing strength of an oscillation with the resonance frequency ω_{0i}; γ_i is parameter that describes damping of such oscillation. The details of the calculation of the dielectric function using Sulforhodamine 101 thin film transmittance can be found in Appendix A as well as basics of the molecular dispersion theory. Besides silver and resin dielectric functions one should include into calculations dielectric permittivities of the prism glass, index matching oil and glass substrate. But in the model these layers are undistinguished and considered as a glass with effective dielectric permittivity ε_g. It has to be noted that parameters ε_S and especially ε_g were varied to get the best overlap of experimental points with calculated data. The new set of parameters A_i, ω_{0i} and γ_i was deduced from the Sulforhodamine 101 resin absorbance data at every step when ε_S was changed. The relation (4.3.1) will not change its form if the wave numbers are used instead of frequencies. Table 4.3.1 contains all parameters that were used in modeling. Thickness of silver is 55 nm, thickness of the Sulforhodamine 101 resin layer is 50 nm. Light is incident from a semi-infinite glass layer (in the experiment the light is incident perpendicularly to air/cylindrical prism interface, so this boundary can be neglected).

Table 4.3.1 The parameters used in reflectance coefficient modeling.

Sample	ε_s	ε_g	A_1	A_2	γ_1, 10^6 m^{-1}	γ_2, 10^6 m^{-1}	ω_{01}, 10^6 m^{-1}	ω_{02}, 10^6 m^{-1}
1	2.5	1.605	0.028	0.00084	1	0.35	10.52	11.45
2	2.7	1.610	0.0365	0.001	1	0.34	10.50	11.42
3	2.9	1.485	0.094	0.0065	1	0.54	10.46	11.4
4	3	1.505	0.133	0.013	1	0.6	10.39	11.33
5	3.1	1.485	0.168	0.019	0.9	0.58	10.38	11.27
6	3	1.33	0.226	0.029	1	0.73	10.38	11.32

One can notice that the parameter ε_g is changing from sample to sample. The possible explanation for this is the compensation of the errors of determination of the angle of incidence.

Also the detection of the scattered radiation was done at detection geometry D2 (figure 4.2.1). The main problem in the scattered radiation measurement is a weakness of the signal. That's why the detector should be brought very close to the sample and the exposure time should be increased significantly. An example of a signal determined at this geometry is shown in figure 4.3.5.

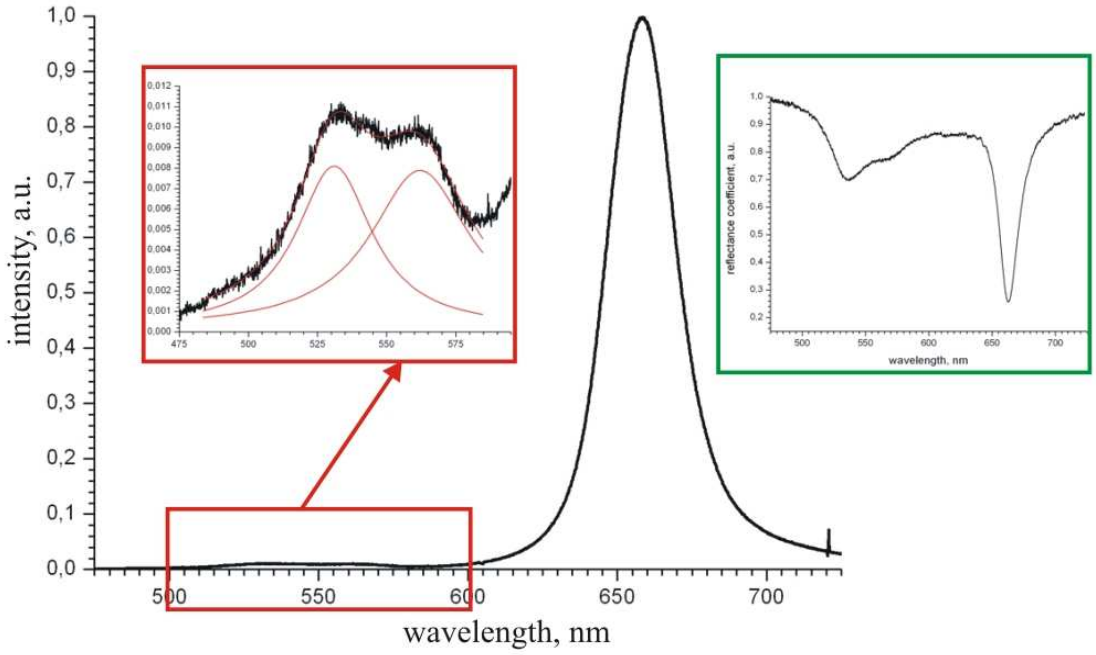

Figure 4.3.5 Normalized intensity of signal determined at geometry D2 for three layers system (Sample 3) is plotted as a function of wavelength (black curve). Angle of incidence is 63º. The inset in the red frame shows zooming of the region of high wavelength peaks. The red curves are fitting lorentzian curves. Inset in the green frame represents the reflectance spectrum of the same sample at the same angle of incidence.

The relation of the signal strength of the low wavelength peak to the signal strengths of the high wavelength peaks is *0.01:0.01:1*. For the comparison one can look at the depth relations of the dips of the reflectance spectrum (inset in figure 4.3.5). It is approximately *0.4:0.3:1*. One could conclude that high frequency SPPs scatter to light less effectively than low frequency ones. The possible reason for that could be higher ohmic losses for SPPs

excited by short wavelength light. The rough estimation of the propagation length of the SPPs is done by using equation

$$L_{SPP} = (2\,\mathrm{Im}[k_x])^{-1} = \mathrm{Im}[\frac{c}{2\omega}\sqrt{\frac{\varepsilon_1 + \varepsilon_2}{\varepsilon_1 \varepsilon_2}}]. \qquad (4.3.2)$$

The results of calculation are summarized in Table 4.3.2. So, the short wavelength SPP (569 nm) travels longer distance before being dissipated to heat than the long wavelength one (*633* nm). It means that the probability to scatter on the film defects to photon is higher for the short wavelength excitation. If the probability of SPP scattering to photon is directly proportional to SPP propagation length, as can be approximated, the ratio of the detected peaks at geometry D2 signal would become *0.4:0.75:1*[*]. But it very clearly contradicts observations.

Table 4.3.2 Estimation of the propagation length of SPPs at silver/ Sulforhodamine 101 resin boundary in sample 3

Wavelength of reflectance coefficient minimum, nm	Propagation length, μm
536	0.97
569	2.50
663	1.03

This contradiction in the theoretical estimation and the experimental observation can be explained by several possible reasons: 1) more precise treatment of SPP's propagation length that takes into account energy dependence of scattering cross section should be used; 2) the propagation length dependence on the metallic film defect density should be taken into account; 2) the energy transfer between the SPP modes could be present. The last one is the most probable reason since the former two reasons seems to be too minor to fully account the big discrepancy. Further studies of the topic will reveal the reason.

[*]The calculation of intensities ratio is done in following way. The coupled intensities are related as *0.4:0.3:1*. The ratio of probabilities to be scattered to photons that are assumed to be proportional to propagation length is approximately *0.4:1:0.4*. After multiplication and normalization one has ration *0.4:0.75:1*

In the figure 4.3.6 two dispersion relations measured at detection 1 and detection 2 geometries for samples with different concentrations of Sulforhodamine 101 are presented. The coupled oscillators model (Section 2.3) is used to fit experimental data.

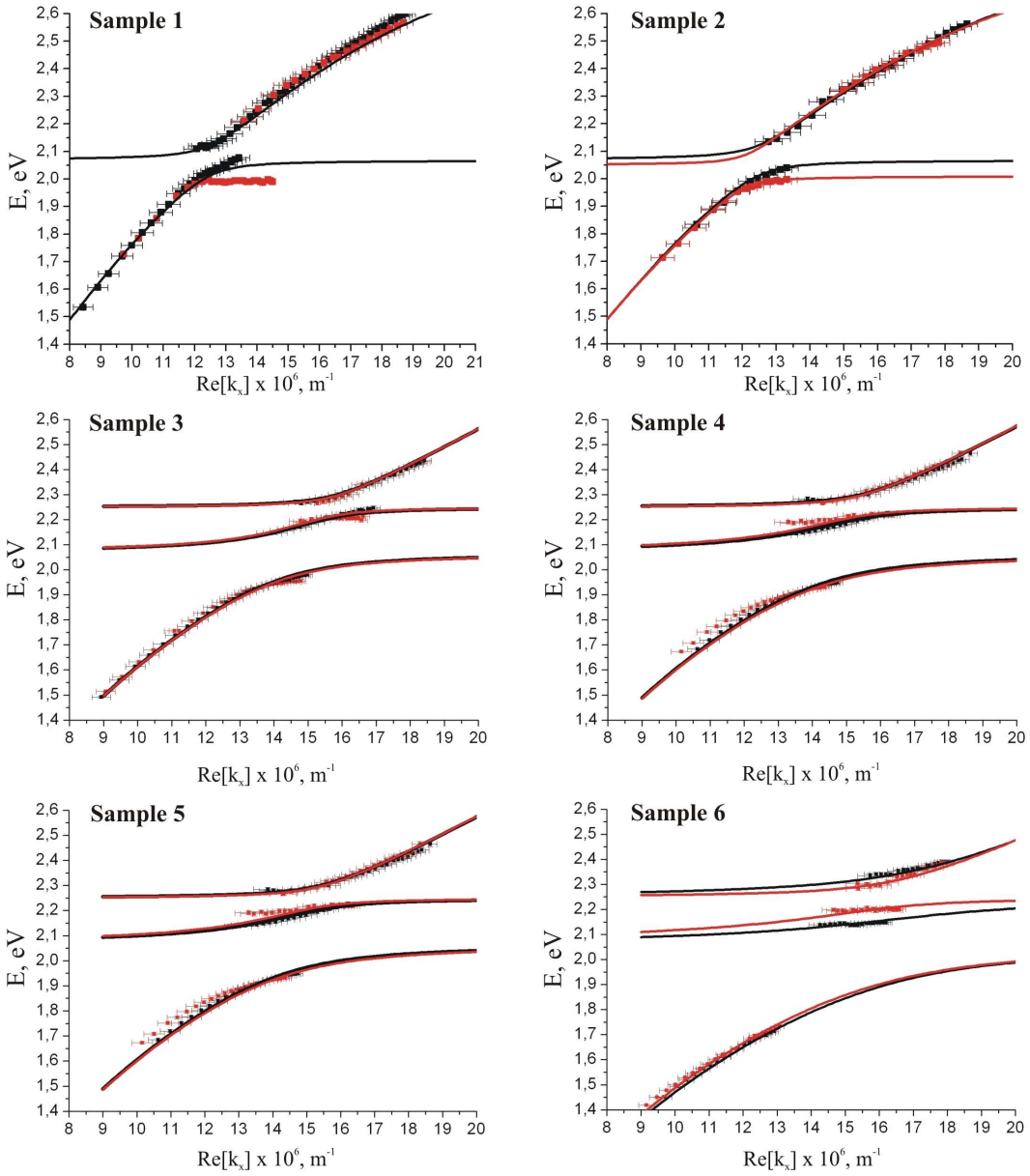

Figure 4.3.6 Dispersion relations of Silver/ Sulforhodamine 101 samples having different dye concentrations. Black dots are measured dispersions at detection geometry D1; red dots correspond to measured dispersion at detections geometry D2. Solid black and red curves represent theoretically calculated dispersion relations for detection 1 and detection 2 geometries respectively using the coupling strengths V_1 and V_2 as fitting parameters.

Detection 1 For the lower dye concentration samples (samples 1, 2) split at the energy corresponding to the absorbance main maximum (2.07 eV) is observed. By further increase of the dye concentration the second split appears at the energy 2.23 eV corresponding to the absorbance shoulder (samples 3-6). According to (1.1), (1.2) and (2.3.22) width of the energy gap is linearly dependent on the square root of the effective oscillator strength. In frame of the Lorentz local field model the relation holds:

$$Nf = \frac{4m_e c\varepsilon_0}{e^2}\frac{9n}{(n^2+2)^2}\int \alpha(v)dv\,, \qquad (4.3.3)$$

where f is an oscillator strength of a single absorber, e and m_e are electron charge and mass, c is the speed of light, ε_0 is the vacuum dielectric constant, N is absorbing molecule concentration, n is the refraction index of the host material (SU-8 matrix), $\alpha(v)$ is the absorption coefficient as a function of incident light frequency. Integral $\int \alpha(v)dv$ is known as a total absorbance and can be calculated straightforward from a measured absorbance. The experimental absorbance spectra are fitted with two lorentzian peaks and the area under the lorentzian curve is directly related to the integral presented in (4.3.3).

Appendix B provides the mechanism of energy gap deduction the from experimental dispersion curves. The obtained lower energy gap behavior is linearly dependent on the square root of total absorbance (figure 4.3.7 a)). The higher energy gap value deduced from the dispersion curves measured at detection geometry D1 also increases with increasing absorbance (figure 4.3.7 b)).

In was checked that with varying irradiance between *0.17-13* W/m^2 the value of Rabi splitting of certain dispersion curve did not change. It means that the condition for vacuum Rabi splitting holds.

Detection 2 The same behavior characterizes dispersion relations obtained from the scattered light detection for samples 3-6. For two lowest dye concentration samples (1, 2) Sulforhodamine 101 fluorescence peak is observed (623 nm), which corresponds to the horizontal part of the dispersion curve. The detected fluorescence can be due to the direct excitation of fluorescent molecules by SPPs. Another indirect rout is possible. SPPs can be scattered into the radiation that can further excite Sulforhodamine 101 molecules.

Detection 2 shows larger values for the lower energy gap in comparison with detection 1 (4.3.7 a)). The linear dependence on the square root of the total absorbance holds for the lower energy gap. However, the upper energy gap is independent on the sample's absorbance and is always close to 125 meV.

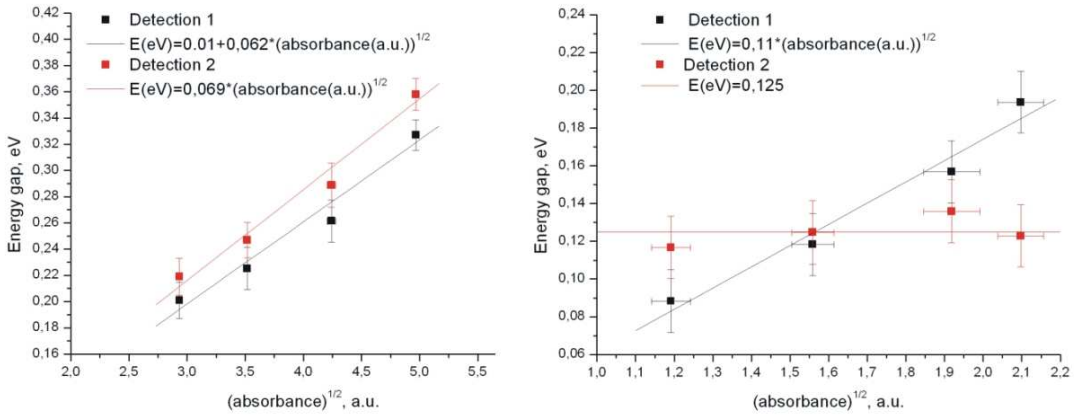

a) b)

Figure 4.3.7 Lower a) and upper b) energy splits as a function of square root of the total absorbance. Black and red lines are linear fits of experimental data.

The observation of linear dependence on square root of Sulforhodamine 101 absorbance can be understood as following. The molecules are interacting with the SPP coherently. In other words SPP induces polarization of the molecules in phase, so as a result the molecules of the sample can be considered as a single high strength oscillator [8]. The number of molecules that takes part in the strong coupling is proportional to the concentration of molecules, i.e., the reference sample absorbance. It is also proportional to the coherence length of SPP, which can be thought as constant in this case. It means that the energy gap is linearly dependent on the square root of total number of molecules in the resin layer.

Let us now use the quantum cavity analogy. As it was written in the introductory part (the equation (1.1)), the value of the Rabi split in the case of cavity photons is

$$E_{Rabi} = 2\hbar[\frac{2\Gamma_0 c N_{qw}}{n_c L_{eff}}]^{1/2} = (\frac{2\hbar^2 e^2 N_{qw}}{n_c^2 \varepsilon_0 m_e L_{eff}})^{1/2} f_{ex}^{1/2}. \qquad (4.3.4)$$

Every parameter in parentheses is essential cavity property and is not dependent on the way the cavity is studied. We adopt this description for the energy gap of the SPP dispersion and

write for the value of the lower energy gap obtained at detection geometry D1 E_{D1}^{L} and detection geometry D2 E_{D2}^{L}

$$E_{D1}^{L} = Af_{D1}^{1/2} + B_1 = A(N_{D1}f)^{1/2} + B_1 \quad (4.3.5.a)$$

$$E_{D2}^{L} = Af_{D2}^{1/2} + B_2 = A(N_{D2}f)^{1/2} + B_2. \quad (4.3.5.b)$$

Here A is a constant coefficient that is dependent on sample properties, f_{D1} and f_{D2} are total oscillators strengths affecting the measurement at detection 1 and detection 2, N_{D1} and N_{D2} are numbers of oscillators that participate in coupling, f is the oscillator strength of an individual molecule (all molecules are assumed to be equal), B_1 and B_2 are contributions to energy due to processes that are not dependent on the total oscillator strength.

In SPP excitation process certain number of molecules N_{D1} was participated. We assume that this number is directly proportional to the total number of molecules N embedded in the dielectric layer, so

$$N_{D1} = \beta_1 N, \quad (4.3.6)$$

where β_1 is a constant. When the SPP propagates and more molecules are excited, the number is still proportional to N

$$N_{D2} = \beta_2 N, \quad (4.3.7)$$

where β_2 is a constant. One can substitute (4.3.6) and (4.3.7) into (4.3.5.a) and (4.3.5.b)

$$E_{D1}^{L} = A(\beta_1 N f_0)^{1/2} + B_1 = (A\beta_1)^{1/2}(Nf_0)^{1/2} + B_1 = C_1(\int \alpha(v)dv)^{1/2} + B_1, \quad (4.3.8.a)$$

$$E_{D2}^{L} = A(\beta_2 N f_0)^{1/2} + B_2 = (A\beta_2)^{1/2}(Nf_0)^{1/2} + B_2 = C_2(\int \alpha(v)dv)^{1/2} + B_2. \quad (4.3.8.b)$$

Here the relation between the total oscillator strength and total absorbance is taken into account, C_1 and C_2 are constants related to that.

As a result of above discussion and the experimentally obtained energy gap vs. total absorbance curve, one can calculate the relative change of the number of oscillators participating into coupling and scattering processes

$$N_{D2} / N_{D1} = \beta_2 / \beta_1 = 0.069 / 0.062 \approx 1.1. \quad (4.3.9)$$

This means that approximately 10% more molecules participate in coupling after initial excitation. The same reasoning can be performed for the upper energy gap

$$E_{D1}^{H} = F(\delta_1 Nf\ )^{1/2} + G_1 = (F\delta_1\ )^{1/2}(Nf\ )^{1/2} + G_1 = K_1(\int \alpha(v)dv)^{1/2} + G_1, \quad (4.4.0.a)$$

$$E_{D2}^{H} = F(\delta_2 Nf\ )^{1/2} + G_2 = (F\delta_2)^{1/2}(Nf\ )^{1/2} + G_2 = K_2(\int \alpha(v)dv)^{1/2} + G_2. \quad (4.4.0.b)$$

Figure 4.3.7. b) shows that $\delta_2 \to 0$. In this model it means that always the same amount of molecules is taking part in coupling while SPP propagates regardless of the concentration. So the SPPs with energies close to the high-energy gap position while propagating do not involve new oscillators, but rather lose them. It can be explained by fast decay of these SPPs to the Joule heat. But examination of the equation (4.3.2) contradicts this possibility. The same conclusions that were done for the signal intensity analysis hold here.

The only question that remains to discuss is the nature of B_1, B_2, G_1 and G_2 energies. As it was mentioned before these parameters can describe contributions to the energy gap by processes that are not dependent on the total oscillator strength or depend on it very weakly. The straightforward explanation to the presence of constant term is calculation of total absorbance with offset. In case of the low energy gap, of *0.01* eV term is most likely due to this fact. But in the case of higher energy gap the situation is different. Experiment reviles that at detection 2 the energy gap remains unchanged with increasing concentration of Sulforhodamine 101. The possible explanation is that modes with energies in higher energy gap region can contain only certain number N_C of oscillating Sulforhodamine 101 molecules. If initially the number of molecules coupled to SPP oscillation were less than N_C, the SPP will propagate and excite more oscillators till their number would be close to N_C. If initially the number of coupled molecules is higher than N_C, during SPP propagation there would be fast decay of excess oscillations to heat or again the possibility of energy transport arises.

However, it is not evident what could be the physical reason for such phenomenon. To gain more insight into the problem let us consider a role of SPP lifetime γ_{SPP}. If the fast energy transfer from high-energy branch to the low-energy branches is taking place, the lifetime of SPP is reduced. So, while the number of molecules is increased during SPP propagation, the reduced lifetime (larger linewidth γ_{SPP}) makes the gap smaller according to (2.3.2).

$$\Delta E = \sqrt{4V^2 - (\gamma_{SPP} - \gamma_{Ex})^2}$$

As it was mentioned at the section 2.3, the energy gap dependence on SPP linewidth is more complex function in the case of SPP interaction with two excitons. But the decrease of the SPP

lifetime may result into the energy gap decrease as it could be seen in figures 2.3.1 and 4.3.8 (the arrow I). The uncertainty relation used to calculate SPP lifetime is written in form

$$\tau_{SPP}(s) \propto \frac{h}{e\gamma_{SPP}(eV)} \tag{4.3.9}$$

The SPP dephasing time is in 10 fs timescale [34].

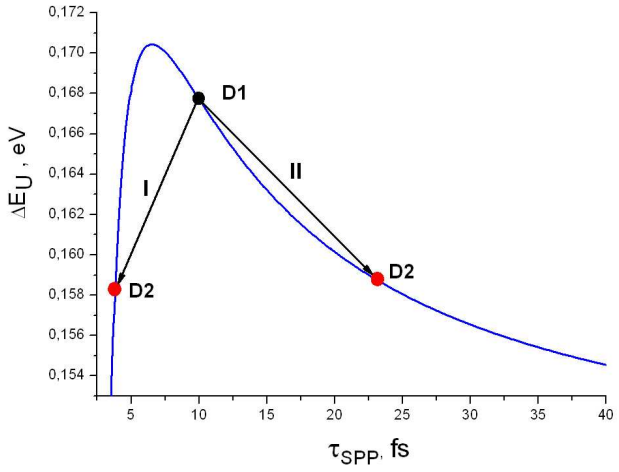

Figure 4.3.8 The upper energy gap dependence on the SPP lifetime. The calculation is done using the coupled oscillator's model in the case of the SPP interaction with two excitons. The black circle indicates the initial lifetime of the SPP mode. The red circles represent the possible SPP lifetime changes. Note that lifetime values (as well as the energy gap values) are used to provide qualitative analysis and might differ from the real values of the SPP lifetime.

Figure 4.3.8 also shows other scenario that leads to the increase of the energy gap value (arrow II). Namely, the increase of the SPP lifetime may occur. Now it is not possible to conclude what is the actual behavior of the SPP/excitons system, because the possibility of the energy transfer between dispersion branches is not studied yet. The only conclusion that can be made now is that the behavior of the upper energy gap value as a function of the square root of the total absorbance is the result of the interplay between two processes. First process leads to increase of the number of oscillators during the SPP propagation and consequently it leads to the increase of the energy gap. The second process results in the SPP lifetime change and decrease of the energy gap value.

5. Summary

In the present work room temperature coherent interaction between the surface plasmon polaritons and Sulforhodamine 101 molecules were studied. Here the achieved goals are summarized.

1. The various approaches to surface plasmon polaritons description and observation are reviewed.
2. Experimental observation of the strong coupling and the vacuum Rabi splitting in planar silver/ Sulforhodamine 101 resin structures is achieved. To do this following steps are covered.
    - 2.1. Sample fabrication techniques are developed.
    - 2.2. Measurements are done in two supplementary detection geometries.
    - 2.3. Experimental data processing methods are developed.
3. The energy gaps dependence on the oscillator strength is analyzed based on the experimental data. The coherent coupling between surface plasmon polariton and dye molecules is proven.
4. Comparison of the results obtained for two detection geometries gave an insight into the dynamics of surface plasmon polariton - exciton interaction.
5. The tasks for future study are realized. The appropriate models for surface plasmon polariton propagation length should be found theoretically and verified experimentally. The study of possible energy transfer between surface plasmon polariton modes should be performed.

References

[1] M.S. Skolnick, T.A. Fisher, D.M. Whittaker, Semicond. Sci. Thecnol. **13**, 645 (1998)

[2] A. Pawlis *et al.*, Microelectron. J. **34,** 439 (2003).

[3] G. Christmann *et al.*, Phys. Rew. B **77** ,085310 (2008).

[4] C.C. Gerry, P.L. Knight, *Introductory Quantum Optics* (Cambridge University Press, 2005).

[5] R. Houdré *et al.*, Phys. Rev. Lett. **73,** 2043 (1994).

[6] D. Baxter *et al.*, Phys. Rev. B **56**, 10032 (1997).

[7] J. Bellessa *et al.*, Phys. Rev. Lett. **93,** 036404 (2004).

[8] T.K. Hakala *et al.*, Phys. Rev. Lett. **103,** 053602 (2009).

[9] D.G. Lidzey *et al.*, Nature **395,** 53 (1998).

[10] R.H. Ritchie, Phys. Rev. **106,** 874 (1957).

[11] H. Raether, *Surface plasmons on smooth and rough surfaces and on gratings* (Springer-Verlag 1988).

[12] M. Fleishmann, P.J. Hedra, A.J. McQuillan, Chem. Phys. Lett. **26,**163 (1974).

[13] T.W. Ebbesen *et al.*, Nature **391,** 667 (1998).

[14] J.B. Pendry, OPN **15,** 33 (2004).

[15] J.R. Krenn, J.C. Weeber Phyl. Trans. R. Soc. Lond. A **362,** 739 (2004).

[16] Q. Wang, J. Wang, S. Zhang, J. Opt. Soc. Am. B **25,** 1096 (2008).

[17] T.K. Hakala *et al.*, Appl. Phys. Lett. **93,** 123307 (2008).

[18] A. Boltasseva, J.Lightw. Technol. **23,** 413 (2005).

[19] H.A. Atwater, J.A. Dionne, H.J Lezec, Science **316,** 430 (2007).

[20] I. Gryczynski *et al.*, Anal. Biochem. **324**, 170 (2004).

[21] S.A. Maier, *Plasmonics. Fundamentals and applications*(Springer 2007).

[22] V.M. Agranovich, M. Litinskaia, D.G. Lidzey, Phys. Rev. B. **67,** 085311 (2003).

[23] R.W. Christy, P.B. Johnson, Phys. Rev. B **6,** 4370 (1972).

[24] B. Harbecke, Appl. Phys. B **39,** 165 (1986).

[25] V.P. Drachev *et al.*, Opt. Express **16,** 1187 (2008).

[26] J. Tignon *et al.*, Phys. Rev. Lett. **74,** 3967 (1995).

[27] A.V. Zayats, I.I. Smolyaninov, A.A. Maradudin, Phys. Rep. **408**, 131 (2005).

[28] I. Gryczynski *et al.*, Anal. Biochem. **324,** 170 (2004).

[29] H. Ditlbacher, Appl. Phys. Lett. **80,** 404 (2002).

[30] R.G. Alargova, Adv. Mater., **16,** 1653 (2004).

[31] G. Wähling, H. Raether, Thin Sol. Films, **58,** 391 (1979).

[32] M.J. Weber, *Handbook of optical materials* (CRC Press 2003).

[33] D.V. Sivuhin *General physics course. Optics* (Nauka 1979).

[34] S.A. Maier *et al.*, Proceedings of SPIE **4810,** 2282 (2002).

Appendix A. Calculation of dielectric permittivity of Sulforhodamine101

To obtain the complex dielectric permittivity of Sulforhodamine 101 as a function of frequency, the classical theory of molecular dispersion was used [33]. In this theory "optical" electrons are considered as damped harmonic oscillator. The oscillations in the electrical field of electromagnetic wave can be described as

$$m\ddot{\vec{r}} = -k\vec{r} - g\dot{\vec{r}} + e\vec{E}\,, \tag{A.1}$$

where m is mass and e is a charge of electron, $-k\vec{r}$ is quazielasticity force, $-g\dot{\vec{r}}$ is an analogous to damping force, which is needed to describe absorption of the molecule and $\vec{E}$ is electric field. (A.1.) can also be written as

$$\ddot{\vec{r}} + 2\gamma\dot{\vec{r}} + \omega_0^2\vec{r} = \frac{e}{m}\vec{E}\,, \tag{A.2}$$

where $\omega_0^2 = \frac{k}{m}$ and $2\gamma = \frac{g}{m}$.

In the case of plane electromagnetic wave, $\vec{E} = \vec{E}_0(\vec{r})\exp(i\omega t)$, after few simplifications and using a definition

$$\vec{D} = \vec{E} + 4\pi\vec{P} = \varepsilon\vec{E}\,, \tag{A.3}$$

one can obtain the expression for the dielectric permittivity in this simplistic case

$$\varepsilon(\omega) = 1 + \frac{4\pi Ne^2/m}{\omega_0^2 - \omega^2 + 2i\gamma\omega}, \tag{A.4}$$

where N is a number of molecules in unite volume. If the molecule has k absorption peaks, one can consider k different oscillators with $m_k, e_k, N_k, \omega_{0k}, \gamma_k$. Such consideration will result in

$$\varepsilon = 1 + \sum_k \frac{4\pi N_k e_k^{\,2}/m_k}{\omega_{0k}^2 - \omega^2 + 2i\gamma_k\omega}\,. \tag{A.5}$$

For dielectric permittivity of Sulforhodamine 101 resin slightly modified formula was used

$$\varepsilon = \varepsilon_s + \sum_k \frac{A_k\omega_{0k}^2}{\omega_{0k}^2 - \omega^2 + 2i\gamma_k\omega} \tag{A.6}$$

where ε_s is dielectric permittivity of the media that is hosting Sulforhodamine 101 molecules and $A_k = 4\pi N_k e_k^{\,2}/\omega_{0k}^2 m_k$.

One can proceed and consider a connection between the dielectric permittivity and the index of refraction

$$\sqrt{\varepsilon} = n - i\kappa, \tag{A.7}$$

where n is real refractive index and κ is a media damping coefficient.

From (A.7) one has

$$\begin{aligned} \mathrm{Re}(\varepsilon) &= n^2 - \kappa^2, \\ \mathrm{Im}(\varepsilon) &= -2n\kappa. \end{aligned} \tag{A.8}$$

Then, using a well-known relation, κ can be written as

$$\kappa = \frac{-\ln(T)\lambda}{4\pi l}, \tag{A.9}$$

where T is a transmittance of a sample of thickness l and λ is a wavelength. The transmittance of 50 nm Sulforhodamine 101 resist films placed on a glass substrate was measured with Perkin Elmer Lambda *850* UV/VIS spectrometer.

Figure A.1 represents $\kappa = \kappa(\omega)$ calculated by (A.8), (A.9) and fitted to an experimental data of a reference sample (50 nm thick layer of resin was deposited on top of the glass substrate). The Sulforhodamine 101 has two absorption peaks, cyclic frequencies around 3.15 and 3.42 THz (or 10.46 x 10^6 and 11.4 x 10^6 m^{-1}) that were obtained from the absorption measurements after fitting the peaks with lorentzian curves. In calculation of $\varepsilon(\omega)$ one has 4 parameters to verify (A_1, A_2) and (γ_1, γ_2). The dielectric permittivity of the SU-8 layer is around 3. For Sulforhodamine 101 resin, to get good overlap with the experimental curve, following parameters were taken $(A_1, A_2) = (0.094, 0.0065)$ and $(\gamma_1, \gamma_2) = (0.3, 0.16)$ THz.

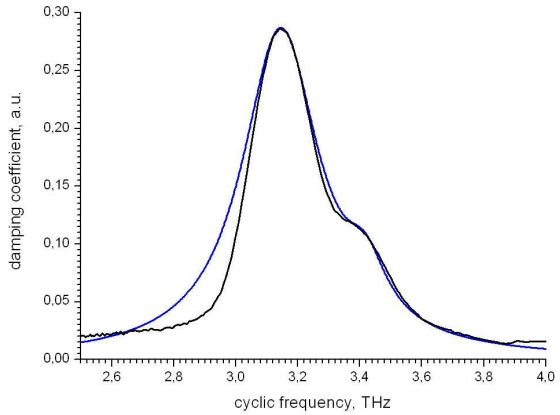

Figure A.1 Experimental (black curve) and theoretical (blue curve) damping coefficient $\kappa = \kappa(\omega)$ of Sulforhodamine 101 resin.

Appendix B. Calculation of the energy gap values

The coupled oscillator model is used to fit the experimentally obtained dispersion relations. In the section 2.3 it was shown that in order to get energy of coupled state, ε, the following equation has to be solved

$$[E_{SPP}(\mathrm{Re}[k_x]) - \varepsilon](E_{Ex1} - \varepsilon)(E_{Ex2} - \varepsilon) - (E_{Ex1} - \varepsilon)V_2^2 - (E_{Ex2} - \varepsilon)V_1^2 = 0\,, \qquad \text{(B.1)}$$

where $E_{SPP}(k_x)$ is an energy of the uncoupled SPP at the interface between silver and dielectric matrix (without absorbing molecules), E_{Ex1} and E_{Ex2} are energies of the excitons, γ_{Ex1} and γ_{Ex2} are linewidths of the excitons, V_1 and V_2 are coupling strengths between the SPP at the silver/dielectric interface and excitons.

Dispersion relation of the uncoupled SPP at the interface between silver and SU-8 resin can be calculated using (2.1.16) or obtained experimentally. In this work the experimentally obtained dispersion relation is used (figure B.1). Energies of the excitons are assumed to be constant and are obtained from experimentally measured absorbance (figure 4.1.4) by fitting its two peaks with two lorentzian curves. V_1 and V_2 are fitting parameters. In order to determine the energy splitting from experimental data, namely the difference in energy between dispersion branches at certain wave vector k_0, the calculated dispersion relation with $V_1 = V_2 = 0$ has to be considered. Such dispersion relation is plotted in figure B.2 a). The wave vector, at which the dispersion branches cross, is marked as $k_{0,1(2)}$.

Next, experimental data are fitted with solutions of (B.1), where V_1, V_2 can be varied to find a good overlap between the experimental and the calculated curves. Energy gap values are defined as

$$\Delta E_L = E_2(k_{0,1}) - E_1(k_{0,1})\,,$$

$$\Delta E_U = E_3(k_{0,2}) - E_2(k_{0,2})\,. \qquad \text{(B.2)}$$

Here $\Delta E_{L(U)}$ is a lower (upper) energy gap value, $E_1(k)$ is an energy of a low energy branch, $E_2(k)$ is an energy of a middle energy branch and $E_3(k)$ is an energy of a high energy branch. The procedure of finding energy splitting is shown schematically in the figure B2.

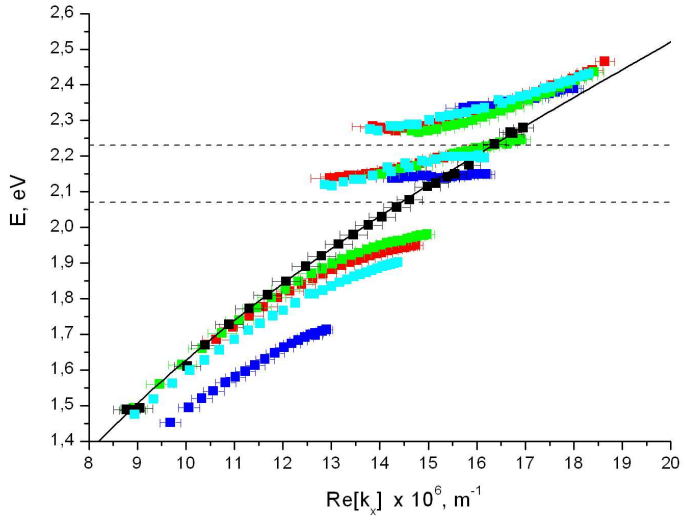

Figure B.1 Dispersion relation of silver (*50* nm)/ SU-8 resist (*50* nm) structure obtained at detection 1 geometry (black dots) together with dispersion relations of silver (*55* nm)/ Sulforhodamine 101 resist (*50* nm) (green dots correspond to sample 3, red dots – to sample 4, light blue dots – to sample 5, blue dots – to sample 6). Solid black line is fitted theoretical curve of silver (*50* nm)/ SU-8 resist (*50* nm) dispersion. Dashed black lines represent energies of absorption maxima and shoulder of Sulforhodamine 101 resin.

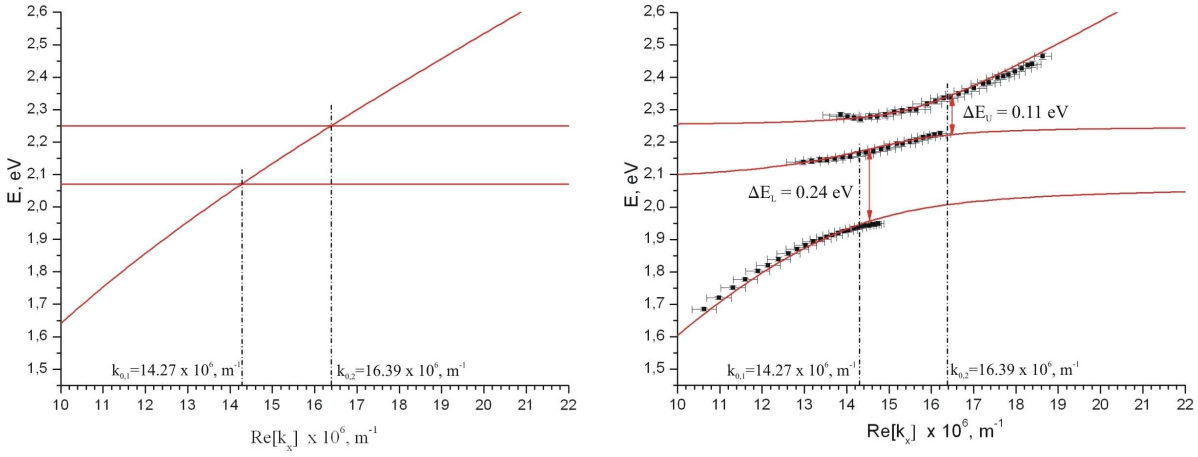

Figure B.2 a) Calculated dispersion relation for silver/Sulforhodamine 101 resin structure, when $V_1=V_2=0$. The wave vectors $k_{0,1}$ and $k_{0,2}$ are determined from the crossing; b) experimentally obtained (black dots) and calculated dispersion relation of the same structure, when V_1=0.12 eV and V_2=0.058eV. Energy gaps ΔE_L and ΔE_U are determined from the calculated dispersions.

Tables B.1 and B.2 contain all parameters that were used in the modeling. Also the table contains information about square root of total absorbance values for lower and higher energy

absorption peaks, $A_L^{1/2}$ and, $A_U^{1/2}$ namely. The parameter a_0 is a multiplier used to alter Silver/SU-8 dispersion relation slope. It is needed in order to get overlap between silver/SU-8 dispersion curve and Silver/SR101 dispersion at the low energy region. Most likely the origin of the discrepancy between two experimental curves is the error in angle of incidence determination or the difference in film thicknesses.

Table B.1 Parameters used in the fitting experimental dispersion relation obtained at detection geometry D1.

№	E_{Ex1}, eV	E_{Ex2}, eV	V_1^{D1}, eV	V_2^{D1}, eV	$A_L^{1/2}$, a.u.	$A_U^{1/2}$, a.u.	a_0	K_{01}, 10^6 m^{-1}	K_{02}, 10^6 m^{-1}	ΔE_L^{D1}, eV	ΔE_U^{D1}, eV
6	*2.06*	*2.25*	*0.15*	*0.12*	*4.97*	*2.10*	*0.95*	*15.66*	*18.17*	*0.33*	*0.19*
5	*2.06*	*2.23*	*0.12*	*0.082*	*4.24*	*1.92*	*1*	*14.38*	*16.42*	*0.26*	*0.16*
4	*2.07*	*2.25*	*0.12*	*0.058*	*3.52*	*1.56*	*1.01*	*14.27*	*16.39*	*0.22*	*0.12*
3	*2.07*	*2.25*	*0.105*	*0.045*	*2.93*	*1.19*	*1.01*	*14.27*	*16.39*	*0.20*	*0.09*

Table B.2 Parameters used in the fitting experimental dispersion relation obtained at detection geometry D2.

№	E_{Ex1}, eV	E_{Ex2}, eV	V_1^{D2}, eV	V_2^{D2}, eV	$A_L^{1/2}$, a.u.	$A_U^{1/2}$, a.u.	a_0	K_{01}, 10^6 m^{-1}	K_{02}, 10^6 m^{-1}	ΔE_L^{D2}, eV	ΔE_U^{D2}, eV
6	*2.06*	*2.25*	*0.17*	*0.075*	*4.97*	*2.10*	*0.95*	*15.66*	*18.17*	*0.36*	*0.12*
5	*2.06*	*2.23*	*0.15*	*0.06*	*4.24*	*1.92*	*1*	*14.38*	*16.42*	*0.29*	*0.13*
4	*2.07*	*2.25*	*0.13*	*0.05*	*3.52*	*1.56*	*1.01*	*14.27*	*16.39*	*0.25*	*0.12*
3	*2.07*	*2.25*	*0.11*	*0.04*	*2.93*	*1.19*	*1.01*	*14.27*	*16.39*	*0.22*	*0.12*